# MODEL BASED FAULT DIAGNOSIS IN ROTOR SYSTEMS

By

N. Ramakrishna Reddy

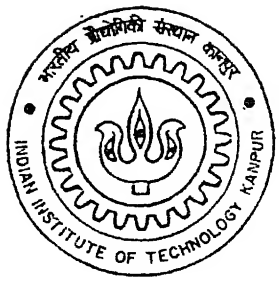


DEPARTMENT OF MECHANICAL ENGINEERING

Indian Institute of Technology, Kanpur

APRIL, 2004

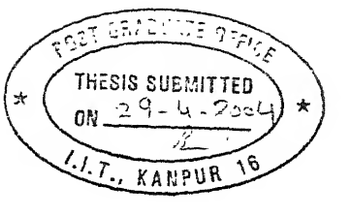


# CERTIFICATE

It is certified that the work contained in the thesis entitled **"Model Based Fault Diagnosis in Rotor Systems."** by *N.Ramakrishna Reddy* has been carried out under my supervision and that this work has not been submitted elsewhere for a degree.

Dr. Nalinaksh S Vyas
(Professor)
Department of Mechanical Engineering,
Indian Institute of Technology, Kanpur.

April, 2004

# ACKNOWLEDGEMENTS

I would like to express my sincere gratitude and thanks to my thesis supervisor Dr. N.S. Vyas for his guidance, invaluable suggestions and constant encouragement. I am also grateful to him for exposing me to the practical aspects vibration diagnostics. I am also thankful to Dr. V. Raghuram for his valuable suggestions, whenever needed..

I am thankful to Prashant Dalawai for his invaluable help, Raghu, Chelladurai for helping me in all possible ways.

I appreciate and extend my sincere thanks to Mr. J.P. Verma and Mr. Mohsin for their untiring help in sorting out hardware problems. I thank all those who have contributed directly or indirectly to my thesis.

Indian Institute of Technology, Kanpur. N.Ramakrishna Reddy

April, 2004.

## Statement of Thesis Preparation

Thesis title "MODEL BASED FAULT DIAGNOSIS IN ROTOR SYSTEMS"

| | | |
|---|---|---|
| 1. | Degree for which submitted | Master of Technology |
| 2. | The thesis guide was referred to for thesis preparation | Yes |
| 3. | Specifications regarding thesis format have been closely followed | Yes |
| 4. | The contents of the thesis were organized according to the guidelines | Yes |

(Signature of Student)
Name: N.Ramakrishna Reddy
Roll No.: Y210520
Department: Mechanical Engg.

# CONTENTS

NOMENCLATURE
LIST OF FIGURES
LIST OF TABLES

1. INTRODUCTION 1
2. LITERATURE REVIEW 4
   2.1 Common faults in Rotating Machinery 5
      2.1.1 Unbalance 5
      2.1.2 Misalignment 6
      2.1.3 Rotor Rub 6
      2.1.4 Rolling Element Bearing Defects 6
      2.1.5 Cocked Rotor 7
      2.1.6 Distortion 8
      2.1.7 Asymmetric Shaft 8
      2.1.8 Mechanical Looseness 8
      2.1.9 Oil Film Whirl 8
      2.1.10 Bending Criticals and Resonance 9
      2.1.11 Gearbox Defects 9
   2.2 Vibration Analysis as a Predictive Maintenance Tool 9
   2.3 Diagnostic Techniques 12
      2.3.1 Time Domain Analysis 12
      2.3.2 Orbital Analysis 13
      2.3.3 Spectrum Analysis 13
      2.3.4 Cepstrum Analysis 14
      2.3.5 Expert Systems 15
      2.3.6 Model Based Diagnosis 15
3. MODEL BASED DIAGNOSIS FORMULATION 16
   3.1 Mathematical Formulation 16

3.2 Finite Element Modeling 17
3.3 Signal Processing Requirements 19
3.4 Determination of Equivalent Loads 19
3.5 Fault Models 20
3.5.1 Unbalance Fault Model 20
3.5.2 Rub 21
3.5.3 Radial and Angular Misalignment 21
3.6 Time Domain Least Square Fitting 23
3.7 Remarks 23
**4. EXPERIMENTAL INVESTIGATIONS 24**
4.1 Experimental Test Rig 24
4.2 Instrumentation 24
4.3 Data Acquisition, Storage and Display 27
4.4 Fault Simulation 31
**5. RESULTS AND DISCUSIONS 38**
5.1 Amplitude Extraction 38
5.2 Experimental Force Vector 41
5.3 Model Force Vector 42
5.4 Unbalance Identification 43
5.5 Radial Misalignment Identification 45
5.6 Angular Misalignment Identification 46
5.7 Rub Identification 48
5.8 Validation 49
5.8.1 Simulation Unbalance at Various Locations on Test Rig 49
5.8.2 Simulation of Radial Misalignment of Various Magnitudes 51
5.8.3..Simulation of Angular Misalignment of Various Magnitudes 52
5.8.4 Simulation of Rub at Various Locations on Test Rig 54
5.9 Remarks 55
**6. CONCLUSIONS AND SCOPE FOR FUTURE WORK 56**

**REFERENCES**

# NOMENCLATURE

| | |
|---|---|
| $\beta$ | Fault vector |
| $\beta_{un}$ | Unbalance fault vector |
| $\beta_{rm}$ | Radial misalignment fault vector |
| $\beta_{am}$ | Angular misalignment fault vector |
| $\Delta M$ | Turning moment |
| $\Delta x(t)$ | Residual displacement |
| $\Delta \dot{x}(t)$ | Residual velocity |
| $\Delta \ddot{x}(t)$ | Residual acceleration |
| $\Delta X_L$ | Magnitude of radial misalignment |
| $\Delta \varphi$ | Magnitude of angular misalignment |
| $\theta$ | Rotational component |
| $\omega$ | Rotational speed |
| [B] | Dampling matrix |
| $D_{ball}$ | Diameter of ball or roller |
| $D_{pitch}$ | Pitch diameter of balls or rollers |
| $E$ | Young's Modulus |
| $E_p$ | Mean square error |
| $F_{bd}$ | Ball Spin defect frequency |
| $F_{cd}$ | Cage defect frequency |
| $F_{ird}$ | Inner race defect frequency |
| $F_{ord}$ | Outer race defect frequency |
| $\tilde{F}$ | Experimental force vector |
| $\tilde{F}_{un}$ | Experimental equivalent force for unbalance |
| $\tilde{F}_{rm}$ | Experimental equivalent force for radial misalignment |
| $\tilde{F}_{am}$ | Experimental equivalent force for angular misalignment |

| | |
|---|---|
| $\tilde{F}_{rub}$ | Experimental equivalent force for rub |
| $F$ | FE model force vector |
| $F_{un}$ | FE model equivalent force for unbalance |
| $F_{rm}$ | FE model equivalent force for radial misalignment |
| $F_{am}$ | FE model equivalent force for angular misalignment |
| $F_{rub}$ | FE model equivalent force for rub |
| I | Moment of inertia |
| $i$ | Node number(Location of fault) |
| [K] | Global stiffness matrix |
| $[K]^{(n)}$ | Elemental stiffness matrix |
| [M] | Global mass matrix |
| $[M]^{l(n)}$ | Elemental stiffness matrix |
| $[M]^{con}$ | Concentrated mass matrix |
| L | Length of Element |
| $RPM$ | Rotational speed |
| $x$ | Displacement vector |

# List of Figures


| Figure | Description | Page |
|---|---|---|
| 3.1 | FE model of rotor system | 18 |
| 3.2 | Finite beam element | 18 |
| 3.3 | Representation of radial misalignment between coupling flanges | 22 |
| 3.4 | Representation of angular misalignment between coupling flanges | 22 |
| 3.5 | Flow chart of identification method | 23 |
| 4.1 | Machinery fault simulator | 25 |
| 4.2 | Instrumentation and data acquisition devices. | 25 |
| 4.3 | Schematic diagram of the experimental set-up and instrumentation | 26 |
| 4.4(a) | Front panel of the data acquisition VI | 28 |
| 4.4(b) | Block diagram of VI | 29 |
| 4.4(c) | MATLAB module | 30 |
| 4.5(a) | Rubbing setup | 32 |
| 4.5(b) | Rubbing kit assembly | 32 |
| 4.5(c) | Individual components of rubbing kit | 32 |
| 4.6 | Time and frequency domain signals for undamaged system | 33 |
| 4.7 | Time and frequency domain signals for unbalance | 34 |
| 4.8 | Time and frequency domain signals for radial misalignment | 35 |
| 4.9 | Time and frequency domain signals for angular misalignment | 36 |
| 4.10 | Time and frequency domain signals for rub | 37 |
| 5.1 | Algorithm for amplitude extraction at running frequency | 39 |
| 5.2 | Residual vibrations $\Delta x(t)$ for various Faults | 40 |
| 5.3 | Residual accelerations $\Delta \ddot{x}(t)$ for various Faults | 41 |
| 5.4(a) | FE Model based equivalent forces | 44 |
| 5.4(b) | Equivalent forces from experimental data | 44 |
| 5.5(a) | FE Model based equivalent forces | 45 |
| 5.5(b) | Equivalent forces from experimental data | 46 |

| | | |
|---|---|---|
| 5.6(a) | FE Model based equivalent forces | 47 |
| 5.6(b) | Equivalent forces from experimental data | 47 |
| 5.7(a) | FE Model based equivalent forces | 48 |
| 5.7(b) | Equivalent forces from experimental data | 49 |
| 5.8 | Validation: Unbalance - Case 1 | 50 |
| 5.9 | Validation: Unbalance - Case 2 | 50 |
| 5.10 | Validation: Unbalance - Case 3 | 51 |
| 5.11 | Validation: Radial misalignment - Case 1 | 52 |
| 5.12 | Validation: Radial misalignment - Case 2 | 52 |
| 5.13 | Validation: Angular misalignment - Case 1 | 53 |
| 5.14 | Validation: Angular misalignment - Case 2 | 53 |
| 5.15 | Validation: Rub- Case 1 | 54 |
| 5.16 | Validation: Rub- Case 2 | 54 |

# List of Tables


| Table | Description | Page |
|---|---|---|
| 2.1 | Identification and correction of malfunction of rotating machinery. | 10 |
| 5.1 | Typical amplitude data (volts) | 40 |
| 5.2 | Experimental force vectors (Newton) | 42 |
| 5.3 | FEM force vectors (Newtons) | 43 |
| 5.4 | Summary of diagnosis for unbalance | 45 |
| 5.5 | Summary of diagnosis for radial misalignment | 46 |
| 5.6 | Summary of diagnosis for angular misalignment | 48 |
| 5.7 | Summary of diagnosis for rub | 49 |
| 5.8 | Summary of validation for unbalance | 50 |
| 5.9 | Summary of validation for radial misalignment | 51 |
| 5.10 | Summary of validation for angular misalignment | 53 |
| 5.11 | Summary of validation for rub | 54 |

# CHAPTER 1

# INTRODUCTION

Vibration of a machine is a major condition monitoring parameter. Vibration signals hold clues to several types of problems and faults, which may occur in a machine. Vibration analysis with appropriate instrumentation can provide reliable knowledge of machine condition. Advances in data acquisition techniques and the developments in the areas of knowledge acquisition, processing and programming make it possible to make the whole process of condition monitoring fully automatic, which would permit early detection of faults than is possible through conventional limits and trend checks.

Rotating machinery fault diagnosis based on vibration measurements calls for reliable data analysis and decision making in the presence of uncertainty. This uncertainty can be attributed to different factors such as measurement of noise, lack of a clear deterministic relationship between the measured quantities and the machine state and variation in the characteristics of the transmission path between the error point and the measurement location due to variations in machine configuration.

Model based monitoring systems give more accurate and faster information than conventional signal based monitoring systems, since a-priori information about the rotor system is systematically included in the identification process. Therefore, the type, position and severity of a fault can be estimated with more reliability and in most cases during the operation without stopping the machine.

For model-based identification of faults, reliable mathematical models of rotor system and possible faults are required. The mathematical models have to be simple so that fast on-line calculations are possible. However, they should also be accurate enough to reproduce the measured vibration s of a real rotor –bearing system.

Exact models of faults are in many cases non-linear. Therefore, time integration algorithms are needed to solve the non –linear equations of the damaged rotor system

directly, although the undamaged system is linear. Such a direct identification of faults would not be possible with this approach.

The new model based method for identification of malfunctions avoids the non-linearities, which are normally brought into the system equations by fault models. This method is based on the idea that, faults can be represented by virtual loads acting on the linear model of undamaged system. Equivalent loads are fictitious forces and moments, which generate same dynamic behavior as the real non-linear damaged system does. System models being originally linear remain linear and unchanged, even if non –linear faults occur. Therefore, to handle the system equations, only simple and fast mathematical procedures are necessary. The identification of the nature, position and severity of faults can be carried out on-line during operation, even if the number of degrees of freedom is very high.

The present study is in continuation of the series of previous works on detection of faults in rotating machinery (Rao, 2001; Padhy, 2002; Ankur, 2003). These works were based on various neural network techniques. Model based diagnosis is an area, which has drawn attention of several researchers (Markert, Plantz, 2001). The focus of the present study is to develop upon some existing analytical model based concepts and implement them for diagnosing rotor faults. Finite Element (FE) technique has been adopted to develop the model. Unlike the signal based monitoring systems, FE model based diagnostic systems developed in recent years utilize all information contained in the continuously recorded vibration signals by taking into account models of the specific machine and possible faults as well as the recorded data of the intact machine. The new method may be used together with or alternatively to conventional signal based monitoring system.

A variety of rotor faults like unbalance, misalignment, and rub are simulated on a Machinery Fault Simulator Rig, in a controlled manner and vibration signals are picked up from multiple stations. Attempt has been made to automate most of the signal processing activities by writing suitable software codes. Data acquisition, time domain display, Fast Fourier Transformation and frequency domain display is done in LabVIEW. Feature extraction from the frequency domain data, and FEM Model codes are written in MATLAB.

A brief review of commonly occurring faults in rotating machinery, their symptoms, and fault diagnosis procedures are discussed in Chapter 2. Model based approach for rotor system and fault models, has been described in Chapter 3. Chapter 4 describes the experimental set-up, methodology used for data acquisition and the typical fault signatures obtained. Feature extraction and results are discussed in Chapter 5. Conclusions and scope for future work are listed in Chapter 6.

# CHAPTER 2

# LITERATURE REVIEW

Fault identification in machinery has been a subject of intensive investigations in the last two decades and several papers have appeared in literature, dealing with many application fields and introducing different methods. Rather complete survey with rich bibliography is reported in reference (Rao J.S, 1996). The identification procedures are generally performed by means of causality correlations of measurable symptoms to the faults. In the area of rotor dynamics, limiting to the most recent contributions, two main approaches can be identified.

In first approach, the symptoms are defined using qualitative information, based on human operator's experience, which creates a knowledge base. Recent contributions include expert systems built up such that different diagnostic reasoning strategies can be applied. Fault-symptom trees, if – then rules or fuzzy logic classification can be used to indicate in a probabilistic approach the type and some times also size and location of most probable fault. Also artificial neural net works (ANN) can be used for creating the symptom fault correlation is given by references (Rao, 2001; Padhy, 2002; Ankur, 2003).

The second approach is quantitative and called as the model based fault detection method. In this approach analytical models of the systems or the processes are used for creating the symptom-fault correlation, or the input-out put relations. However this method has many different ways of application. Among recent contributions available in literature researchers introduce a fuzzy clustering method in which the basis to consider the vibration data as a high dimension feature vector and vibration caused by a particular fault on a specific machine can be considered to be a point in this high dimension space. The same fault, on a number of similar machines, should produce a cluster of points in the high dimension space that is distinct from other cluster produced by different faults. The main drawback of this method is the availability of large database of dynamic

behavior of similar machines, which can emphasize the differences in the response of similar machines.

In other applications, fault detection can be performed by means of different model-based approaches according to the nature of the system under observation:

- Parameter estimation, when the characteristic constant parameters of processes or of the components are affected by the fault.
- Static estimation, when the constant parameters are unaffected by possible faults and only the state of the system, which is represented by set of generally un measurable state variables (function of time), is affected by faults; in this case the model acts as a state observer.
- Parity equation, when the faults affect some of the immeasurable input variables, the parameters are constant, and only output variables compared with calculated out put variables.

Therefore, the fault can be identified from parameter or state estimation or from parity equation.

## 2.1 Common Faults in Rotating Systems

The most common problems are generally related to *ABC* category Eishleman (1998) – Alignment, Balance and incorrect Clearances (typically on bearings). Prominent rotating machinery problems include – Unbalance, Misalignment, Rolling Element Bearing Defects (Outer Race Defect, Inner Race Defect, Ball Spin Defect, and Train/Cage Defect), Cocked Rotor, Rub, Casing Distortion, Asymmetric Shaft, Mechanical Looseness, Oil Film Whirl, Bending Resonance: Gearbox Defects, etc. Both experimental and analytical techniques are routinely used for diagnosis of faults. The most prominent types of rotating machinery problems are discussed below along with the causes and symptoms.

### 2.1.1 Unbalance

Unbalance is the single most prominent problem of a rotor system that may cause the entire machine to vibrate excessively. This in turn may cause excessive wear in bearings, bushings, shafts, gears, cabling, hoses, cowlings and exhaust systems substantially

reducing their service life. When rotation begins, the unbalance exerts centrifugal force tending to vibrate the rotor and its supporting structure. The higher the speed, the greater is the centrifugal force exerted by the unbalance and more violent is the vibration. Centrifugal force increases proportionally to the square of the increase in speed. If the speed doubles, the centrifugal force is quadrupled, etc. Vibration due to unbalance prominently occurs at a frequency equal to the rotor speed. However, specific unbalance forces caused as in the case of ball bearing wear give rise to additional characteristics like high frequency signals corresponding to bearing vibration frequency.

### 2.1.2 Misalignment

In very broad terms, shaft misalignment occurs when the centerlines of rotation of two (or more) machinery shafts are not in line with each other. In more precise terms, shaft misalignment is the deviation of relative shaft position from a collinear axis of rotation measured at the points of power transmission when equipment is running at normal operating conditions. The misalignment of shafts and other components is one of the most common causes of vibration and failures. Misalignment is present in almost every machine to some extent. Coupling misalignment causes friction and deflection forces, which cause the rotor bearing system to deflect, creating secondary phenomena such as harmonic resonances. Frequencies are characteristically twice the running speed, but first and sometimes third or fourth multiples of running speed is also observed. Misalignment can be classified as parallel or angular.

### 2.1.3 Rotor Rub

The physical contact between rotating elements and stationary machine parts can generate rub condition. Rub can be radial or axial. Mechanical seal rub is a typical example of radial rub, while casing rub at shaft end is a case of axial rub. Mostly both the types of rubs generate vibration at frequency equal to twice the rotational frequency but lower and higher frequencies are also common.

### 2.1.4 Rolling Element Bearing Defects

The commonly used of rolling element bearings types are ball bearings, roller bearings, tapered roller bearings, needle bearings. These contain elements that roll between an

inner race and an outer race with very close clearances. They provide high stiffness to the rotor but are low in damping. Rolling element bearings have very limited life so it is desirable to monitor these bearings for early indication of impending failure. Application of high loads, shock loads, or bearing attrition due to extended run times increase the internal clearances resulting in bearing failure. Typically four types of defects are observed in rolling element bearings, each giving rise to vibrations at a specific frequency. Each defect excites causes vibrations at different frequencies which are related to the bearing geometry as described next:

| Type of Defect | Frequency | |
|---|---|---|
| Outer Race Defect | $F_{ord} = \left\{\frac{N}{2}\right\} \times \left\{1 + \left(\frac{D_{ball}}{D_{pitch}}\right) \times Cos\beta\right\} \times RPM$ | (2.1) |
| Inner Race Defect | $F_{ird} = \left\{\frac{N}{2}\right\} \times \left\{1 - \left(\frac{D_{ball}}{D_{pitch}}\right) \times Cos\beta\right\} \times RPM$ | (2.2) |
| Ball Spin Defect | $F_{bd} = \left(\frac{1}{2}\right) \times \left\{\left(\frac{D_{pitch}}{D_{ball}}\right) - \left(\frac{D_{ball}}{D_{pitch}}\right) \times (Cos\beta)^2\right\} \times RPM$ | (2.3) |
| Train/Cage Defect | $F_{cd} = \left(\frac{1}{2}\right) \times \left\{1 - \left(\frac{D_{ball}}{D_{pitch}}\right) \times Cos\beta\right\} \times RPM$ | (2.4) |

where,

$N$ = Number of contained balls or rollers

$RPM$ = Rotational speed of bearing inner race (Hz)

$D_{ball}$ = Diameter of ball or roller

$D_{pitch}$ = Pitch diameter of balls or rollers

$\beta$ = Bearing load contact angle (degrees)

### 2.1.5 Cocked Rotor

A rotor with its plane not perpendicular to axis of rotation is termed cocked. Also, unevenness in mass distribution on either side of the plane perpendicular to rotational axis and passing through geometric center of the rotor produces cockiness. This fault generates excessive vibration in axial direction prominently at the first multiple of rotational frequency. Sometimes, second or third multiples of rotational frequency is also observed.

### 2.1.6 Distortion

Casing and foundation distortion cause vibration in an indirect way, either by generating misalignment between driver and driven machines or by causing internal rub or uneven bearing contact. This in turn transmits forces to the rotor, inducing it to generate forces of its own, such as unbalance and a wide variety of oil film and friction induced forces. Another possibility is that the loads on casing supports shift and can set off a series of resonance problems. Piping forces and foundation distortion often cause this type of difficulty.

### 2.1.7 Asymmetric Shaft

The response of the asymmetric shaft has several harmonics and the frequencies observed are first, second or third multiples of the rotational frequency and sometimes even higher harmonics, if the asymmetry is predominant.

### 2.1.8 Mechanical Looseness

Loose rotor components such as disks, sleeves, thrust collars etc. cause internal friction problems. The frequency of vibration is always the rotor critical speed. Mechanical loose components like bolts give rise to $1\times rev$ and harmonic frequency signals due to secondary phenomena. The amplitude and phase continually change. Loose assembly of bearings give rise to sub-harmonic response and the typical frequency response is $0.5\times rev$ and $(1/3)\times rev$. This could be mistaken for oil film whirl, particularly in the region of twice the rotor critical speed, around the threshold of instability.

### 2.1.9 Oil Film Whirl

Oil whirl in an oil lubricated journal bearing can occur due to preload forces, shaft/bearing conditions, shaft eccentricity/concentricity or initial rotor deflection. In such an eventuality a flowing wedge of oil forms in the bearing and drives the shaft ahead of its forward circular motion within the bearing clearance. The frequency of response at the onset of the whirl is always a little less than $0.5x$ *rev,* in the region of 0.4 to $0.5x$ *rev.* Generally it occurs around 0.45 to $0.48x$ *rev.* The frequency gets locked at the critical speed in the unstable region, if the whip is severe. If the bearing is damaged, high frequency response will be observed, due to the rubbing of debris.

### 2.1.10 Bending Criticals and Resonance

Bending critical of the rotor occurs when the rotational speed is equal to its lateral resonance frequency. Bending critical can be easily detected by synchronous whirl conditions and fairly large amplitude at the rotor speed. Unlike resonance frequency, the critical speed cannot be cured by addition of damping, which in fact may be harmful, causing internal hysteresis. Resonance of the structure, support and auxiliaries cause fairly large amplitudes of vibration at the rotor speed and this occurs over a narrow range of speed of operation. Such resonance can be cured by the addition of damping.

### 2.1.11 Gearbox Defects

Gearboxes generate additional frequency components equal to running speeds of various shafts associated with them. Also, gear teeth meshing frequencies are prominent. Defects in any of the shafts show frequency components as multiples of the rotational frequency of that shaft. Gear teeth damage/break off show higher amplitudes at gear teeth meshing frequency.

A summary of the rotating machinery defects, characteristics and common remedial measures are given in Table 2.1.

## 2.2 Vibration Analysis As a Predictive Maintenance Tool

Various maintenance techniques can be broadly classified in the following manner as Corrective Maintenance, Preventive Maintenance, and Predictive Maintenance. Corrective Maintenance involves replacement of defective parts of a machine once it has been observed to function irregularly. This technique is also commonly referred to as Breakdown Maintenance which means if it broken - fix it! And can only be used for non-critical machinery. With plant downtime becoming more expensive, a failure could be quite expensive in lost production time, and thus preventative maintenance evolved. This involves regular inspections and overhauls at predetermined intervals.

Table 2.1 Identification and correction of malfunction of rotating machinery

| Fault | Frequency | Spectrum; Time-domain, Orbit shape | Correction |
|---|---|---|---|
| Mass unbalance | 1X | Distinct 1X with much lower values of 2X, 3X, etc., elliptical and circular orbits | Field or shop balancing |
| Misalignment | 1X, 2X, etc., | Distinct 1X with equal or higher values of 2X, 3X, etc., | Perform hot / cold alignment |
| Shaft bow | 1X | Dropout of vibration around critical speed in Bode plot | Heating or peening to straighten rotor |
| Steam loading | 1X | Load sensitive 1X | Modify admission sequence: repair diaphragms: reinstall nozzles blocks |
| Bearing wear | 1X, sub harmonics, orders | High 1X, high 0.5X, sometimes 1.5 or orders; cannot be balanced | Replace bearing |
| Gravity excitation | 2X | 0.5 critical speed appears on Bode plot | Reduce eccentricity by balancing |
| Cracked rotor | 1X, 2X | High 1X,0.5 critical speeds may show upon coast-down | Remove rotor |
| Looseness | 1X plus large number of orders, 0.5X may show up | High 1X with lower-level orders, large 0.5 order | Shim and tighten bolts to obtain rigidity |
| Coupling lockup | 1X, 2X, 3X. etc., | 1X with high 2X similar to misalignment; may yield different vibration patterns | Replace coupling or remove sludge |
| Thermal instability | 1X | 1X has varying phase angle and amplitude | Compromise balance or remove problem |
| Oil-Whirl | 0.35X-0.47 X | Sub synchronous component less than 0.5 order informal loop in orbit | Temporary: load bearing heavier, correct misalignment; long term: change brg. type |
| Oil-Whip | fn1 | Sub synchronous component does not change with speed | Change bearing type |
| Sub harmonic resonance | 0.5X, 1/3X, 0.25X, and higher | Sub synchronous Vibration depending on natural frequency | Remove looseness, excessive flexibility; change natural frequency so it does not match fractional frequencies |
| Hysteresis | 0.65X to 0.85X | High-magnitude fractional frequency (greater than 0.5x) | Eliminate or secure built-up parts |
| Rubs | 0.25X, 1/3X, 0.5X | External loops in orbit | Eliminate rub causing conditions as thermal bow and mass unbalance |
| Trapped Fluid | 0.8X to 0.9X | Bearing-sum and different frequencies | Remove fluid in rotor if possible; otherwise eliminate 1X component |

1X=One time operating speed. fn1=First natural frequency

An efficiently planned preventive maintenance program can be quiet effective in discovering the faults in a machine before they reach a terminal state. The main drawback of this method is machines are overhauled while they are still in good condition, and it turns out to be an expensive method. This is also sometimes referred to as PPM (Planned Preventive Maintenance). With the development of condition monitoring techniques, methods were available to determine the actual condition of the machine, and even calculate the time to failure. This enables planners to overhaul a machine when it needed it, and to concentrate on the problem areas. This is known as predictive maintenance. Predictive Maintenance techniques have gained prominence in the last decade.

Some of the benefits from a predictive maintenance program are: (i) early warning of problems allows correction without overtime, with minimal impact to production, and without high expediting costs to procure replacement parts; (ii) elimination of unexpected failures which create extensive, costly repairs and expensive loss of production, whereas early correction would have been inexpensive; (iii) effective scheduling of the maintenance workforce during outages to concentrate on the equipment most in need of repair; (iv) extended maintenance intervals for those machines with healthy vibration signatures; (v) isolating the cause of problems without resorting to shot gunning of the solution; (vi) no capital expenditure or staff involvement is necessary - we do everything required; (vii) no modification to machines or disruption to production.

Various Predictive Maintenance techniques include temperature monitoring, current and voltage monitoring, metallurgical failures analysis, oil analysis, wear debris analysis (e.g. ferrography, atomic absorption, atomic emission, etc.), infrared thermography as well as vibration and sound analysis. In the case of rotating machinery (such as industrial turbines, motors, pumps, fans or gearboxes), Vibration Analysis has become the most popular Predictive Maintenance technique, as the vibration signals measured at critical points on the external surface of a machine (for example, a ball bearing) can contain vital information about the internal processes, and can produce valuable information about the state of development of different possible faults, like machine unbalance, axis misalignment, ball bearing and gear related faults, eccentricities or mechanical looseness.

## 2.3 Diagnostic Techniques

Experimental and analytical techniques, both, have been routinely used for diagnosing faults in operational rotating machinery. These techniques are also used during the design and development processes. Some of these diagnostic techniques are discussed below.

### 2.3.1 Time Domain or Wave Form Analysis

Time domain signal is an unprocessed record of the vibration as picked up from a transducer. It consists of information about the physical behavior of machine. A serious limitation is that it can be too complex for analysis if excessive noise, signal modification or several frequencies are present. Several magnitude parameters can be extracted from the time history of a noise or vibration signal. They are (i) the peak level (ii) root mean square (rms) level and (iii) the crest factor. Crest factor is the ratio of the peak level to the rms level. It is a measure of the impulsiveness of a noise or vibration signal. In addition to peak levels, rms levels and crest factors, various other statistical parameters can be extracted from the time histories of the noise and vibration signals. These include (i) Probability density distributions, (ii) second, third and fourth order statistical moments. The first two statistical moments of a probability density distribution are the mean value and the mean square value. The third statistical moment is the skewness of a distribution and it is a measure of the symmetry of the probability density function. The fourth statistical moment is widely used in machinery diagnostics, particularly for rolling element bearings. It is called kurtosis. The kurtosis of a signal is very useful for detecting the presence of an impulse within the signal. It is widely used for detecting discrete impulsive faults in rolling element bearings. Good bearings tend to have a kurtosis value ~3, and bearings with impulsive defects tend to have higher values (generally>4). The usage of the kurtosis is limited because, as the damage to a bearing becomes distributed, the impulsive content of the signal decreases with a subsequent decrease in the kurtosis value. However, the time domain data is normally too difficult to analyse in such form as signals are not always periodic and are mostly polluted by noise. Noise can be reduced by signal conditioners but cannot be eliminated altogether. Time between events represents the frequency component specific to the machine.

### 2.3.2 Orbital Analysis

The horizontal and vertical motions of the rotor with respect to a sensor mounted on the bearing are simultaneously displayed on oscilloscope. The orbit represents the instantaneous position of the rotor. The orbit can be used to assess oil whirl and other asynchronous motions as well as synchronous phenomena such as mass unbalance and misalignment. Orbital analysis is also employed to diagnose problems like shaft pre-loading. For example, a horizontal pre-load (e.g. misalignment) restricts horizontal motion and will produce an elliptical orbit with the vertical axis longer than the horizontal. Other defects like torque reaction, pressure angle forces associated with gearboxes, internal seal rub due to casing distortion, shaft rubs etc. can also be studied through orbital analysis.

### 2.3.3 Spectrum Analysis

It is common for information to be encoded in the sinusoids that form a signal. The information on frequency, phase and amplitude of the component sinusoids is obtained from the DFT (Digital Fourier Transform) or the FFT (Fast Fourier Transform). The FFT spectrum of a signal can be obtained by standard digital FFT algorithms. Vibration signals of rotating machinery mainly comprise of peaks at the machine's rotating frequency (RF) and its harmonics (2xRF, 3xRF, 4xRF). The magnitudes of some of these peaks vary considerably in presence of faults. For example, the spectrum of a machine with mass unbalance will normally show a clear peak at the rotating frequency, while in a misaligned machine the second harmonic of the rotating frequency is usually particularly excited. On the other hand, if a defect appears in one of the ball bearings like for example a small irregularity in the bearing's outer race, inner race, or one of the rolling elements, vibration occurs at frequencies bearing specific relationships with the bearing geometry. Other types of peaks that can be observed in the frequency domain are side bands of the bearing defect frequencies with the rotating frequency. The appearance of side bands in the power spectrum is an effect of the modulation of a signal with frequency $f_1$ by another signal with frequency $f_2$. If, for instance, the periodic signal cos $(2\pi f_1)$ is modulated by the signal cos $(2\pi f_2)$, the resulting signal will be cos $(2\pi f_1)$ *cos* $(2\pi f_2)$. The power spectrum of such a signal consists of two peaks at frequencies $(f_1 + f_2)$ and $(f_1 - f_2)$ frequencies.

### 2.3.4 Cepstrum Analysis

Cepstrum is the forward Fourier transform of a spectrum. It is thus the spectrum of a spectrum, and has certain properties that make it useful in many types of signal analysis. One of its more powerful attributes is the fact that any periodicities, or repeated patterns, in a spectrum will be sensed as one or two specific components in the cepstrum. If a spectrum contains several sets of sidebands or harmonic series, they can be confusing because of overlap. But in the cepstrum, they will be separated in a way similar to the way the spectrum separates repetitive time patterns in the waveform. Gearboxes and rolling element-bearing vibrations lend themselves especially well to cepstrum analysis. The cepstrum is closely related to the auto correlation function. The word cepstrum was coined by reversing the first syllable in the word spectrum. The cepstrum exists in a domain referred to as quefrency (reversal of the first syllable in frequency), which has units of time. The real cepstrum of a digital signal x(n) is defined as:

$$c(n) = \frac{1}{2\pi} \int_{-\pi}^{\pi} \ln |X(\omega)| e^{j\omega n} d\omega \tag{2.5}$$

and the complex cepstrum is defined as:

$$\hat{x}(n) = \frac{1}{2\pi} \int_{-\pi}^{\pi} \ln |X(\omega)| e^{j\omega n} d\omega \tag{2.6}$$

where the complex logarithm is used:

$$\hat{x}(\omega) = \ln X(\omega) = \ln |X(\omega)| + j\theta(\omega) \tag{2.7}$$

$$\theta(\omega) = \arg(X(\omega)) \tag{2.8}$$

The power cepstrum can be used for the identification of any periodic structure in a power spectrum. It is ideally suited to the detection of periodic effects such as detecting harmonic patterns in machine vibration spectra- e.g. the detection of turbine blade failures, and for detecting and separating different side band families in a spectrum- e.g. gear box faults. Power cepstrum analysis is generally used as a complementary tool to spectral analysis. It helps identify items, which are not readily identified by spectral analysis. Its main limitation is that it tends to suppress information about the over all spectral content of a signal, spectral content, which might contain useful information in

it's own right. It is thus recommended that cepstrum analysis always be used in conjunction with spectral analysis. Another type of cepstrum, which is sometimes used in signal analysis, is the complex cepstrum. The complex cepstrum is defined as the inverse Fourier transform of the logarithm of the forward Fourier transform of a time signal.

### 2.3.5 Expert Systems

Conventional manual trend checking methods and diagnosing often require human experts to analyze the vibration signature. In Expert Systems attempt is made to develop an algorithm on the basis of human expertise, which is available. These are often considered to be one of the most popular application of artificial intelligence (AI). Knowledge base is the most important part of any expert system. It is stored in the form of facts and rules. The facts are termed as deep knowledge and rules are simply the heuristics. The knowledge is controlled by an inference engine, which interacts with the user and the knowledge base according to the rules contained in it. Since the knowledge or data in most cases may be incomplete or uncertain, the models employ probabilistic reasoning technique such as Bayes's rule, fuzzy logic, Dempster-Shafer calculus etc.

### 2.3.6 Model Based Diagnosis

In one of the major works, (Markert et al., 2001) presented a model in which equivalent loads due to the faults are virtual forces and moments acting on the linear undamaged system model which generate a dynamic behavior that is identical to the measured one of the damaged system. The identification is then performed by least-square method in time domain. (Markert et al., 2001) later employ least square method for identifying various faults. In this model-based identification procedure, the input variables are the exiting forces and out put variables are the vibrations .The procedure requires the model definition of elements (rotors, bearings) that compose the rotor system .A finite beam element model is assumed for the rotor.

In this present study method the model-based procedure is developed upon and implemented for a rotor-bearing test system.

# CHAPTER 3

# MODEL BASED DIAGNOSIS FORMULATION

The Model based diagnosis approach is based on the idea that, faults can be represented by virtual loads acting on the model of the undamaged system. Equivalent loads are fictitious forces and moments, which generate the same dynamic behavior as the real damaged system does. The identification of the nature, location and severity of the fault is done through analyses of these virtual forces.

## 3.1 Mathematical Formulation

The model of the undamaged system can be taken as linear. An N degrees of freedom system can be described by (Markert et al., 1997; Markert, Siedler and Platz., 2001)

$$[M]\{\ddot{x}_0(t)\}+[C]\{\dot{x}_0(t)\}+[K]\{x_0(t)\}=\{F_0(t)\} \tag{3.1}$$

Where $F_0(t)$ is the load acting on the system during normal operation; $x_0(t)$ is the N-dimensional displacement vector; $[M]$, $[B]$ and $[K]$ are the mass, damping and stiffness matrices of undamaged system.

Occurrence of a fault changes the system properties which may result in a response $x(t)$, different from the normal vibration $x_0(t)$. The differences between the vibrations $x(t)$ of damaged system and the normal vibrations $x_0(t)$ of undamaged system are residual displacements, residual velocities and residual accelerations, respectively given by

$$\begin{aligned}\Delta x(t) &= x(t)-x_0(t)\\ \Delta\dot{x}(t) &= \dot{x}(t)-\dot{x}_0(t)\\ \Delta\ddot{x}(t) &= \ddot{x}(t)-\ddot{x}_0(t)\end{aligned} \tag{3.2}$$

The magnitude of these residues depends on fault vector $\beta$, which describes the fault parameters like type of fault, magnitude of fault and location of fault. For example, magnitude of unbalance $u_i$ and its location $i$ describes an unbalance.

These residual vibrations $\Delta x(t)$ can be imagined to be caused by additional time varying forces $F(\beta,\ddot{x},\dot{x},x,t)$ acting on the undamaged system, equation (3.1), i.e.

$$[M]\{\ddot{x}(t)\}+[C]\{\dot{x}(t)\}+[K]\{x(t)\}=\{F_0(t)\}+\left\{\tilde{F}(\beta,\ddot{x},\dot{x},x,t)\right\} \tag{3.3}$$

Subtraction of the equations of motion of the undamaged system (3.1), from the equations of motion for damaged system (3.3) yields

$$[M]\{\Delta\ddot{x}(t)\}+[C]\{\Delta\dot{x}(t)\}+[K]\{\Delta x(t)\}=\left\{\tilde{F}(\beta,\ddot{x},\dot{x},x,t)\right\} \tag{3.4}$$

The above equation relates measured residual vibrations directly to the equivalent forces of faults present in the system.

Computation of the equivalent load, $\tilde{F}(\beta,\ddot{x},\dot{x},x,t)$, which represents the fault arising in the rotor system, requires measurements $x_0(t)$ on the normal system, measurements $x(t)$ on the system with fault and the system properties $[M],[C],[K]$. The mass and stiffness matrices are computed through a finite element model. Damping is ignored in this study.

## 3.2 Finite Element Modeling

The present study is carried for a rotor bearing system. It is considered to be a far coupled system and is modeled through linear 2D finite beam elements. Each node has two degrees of freedom (d.o.f), namely $x$ and $\theta$. The FE model of rotor system is shown in Fig. 3.1. Each element is represented by two degrees of freedom at a node as shown in Fig. 3.2.

The elemental stiffness matrix for beam element is given by

$$[K]^{(n)}=\frac{EI}{L^3}\begin{bmatrix} 12 & 6L & -12 & 6L \\ 6L & 4L^2 & -6L & 2L^2 \\ -12 & -6L & 12 & -6L \\ 6L & 2L^2 & -6L & 4L^2 \end{bmatrix} \tag{3.5}$$

The global stiffness matrix *[K]* is obtained by assembling all elemental stiffness matrices.

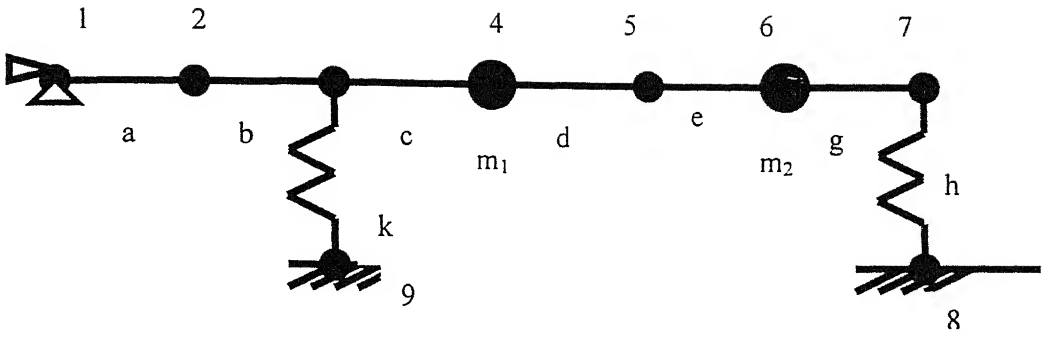


1, 2, 3, 4, 5, 6, 7, 8, 9 are the Node Numbers
a, b, c, d, e, g, h, k are the Element Numbers
$m_1$ and $m_2$ are the masses of disks

**Fig. 3.1 FEM model of rotor system**

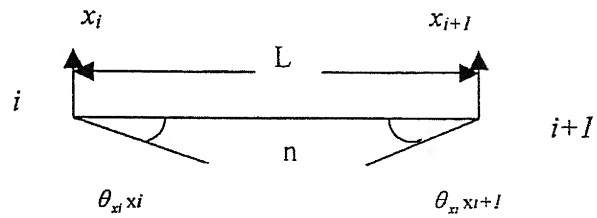


$x_i$ and $x_{i+1}$ are the displacements in X-direction,
$\theta_{xi}$ and $\theta_{xi+1}$ are the slopes in X-direction,
*ii* and $i+1$ are two successive nodes,
n is element number,

**Fig. 3.2 Finite beam element**

The elemental mass matrix is given by

$$[M]^{1(n)} = \begin{bmatrix} 156 & 22L & 54 & -13L \\ 22L & 4L^2 & 13L & -3L^2 \\ 54 & 13L & 156 & 22L \\ -13L & -3L^2 & 22L & 4L^2 \end{bmatrix} \tag{3.6}$$

The global mass matrix $[M]^1$ is obtained by assembling all elemental mass matrices.

The rotor model has two discrete disks. The consequent concentrated mass matrix can be written as

$$[M]^{con}=\begin{bmatrix} m_1 & 0 & 0 & 0 \\ 0 & 0 & 0 & 0 \\ 0 & 0 & m_2 & 0 \\ 0 & 0 & 0 & 0 \end{bmatrix} \tag{3.7}$$

The overall mass matrix $[M]$ is sum of global mass matrix $[M]^l$ and concentrated mass matrix $[M]^{con}$

$$[M]=[M]^l+[M]^{con} \tag{3.8}$$

## 3.3 Signal Processing Requirements

The identification process requires displacement, velocity and acceleration data on every measurement position of rotor system. These can be measured using appropriate types of transducers. However, only one parameter e.g. displacement can be obtained experimentally and the other two can be mathematically computed by differentiation of displacement signal.

It should be noted that for calculating the residual vibrations, measured vibration data for both the undamaged and the damaged rotor system have to be available for the same operating and measurement conditions, e.g. rotor speed and sampling frequency.

## 3.4 Determination of Equivalent loads

The equivalent force $\tilde{F}(t)$ characterizing the unknown faults is calculated by putting the residuals accelerations $\Delta\ddot{x}(t)$, residual velocities $\Delta\dot{x}(t)$ and residual displacements $\Delta x(t)$ of full vibration state into equation (3.4)

$$[M]\{\Delta\ddot{x}(t)\}+[C]\{\Delta\dot{x}(t)\}+[K]\{\Delta x(t)\}=\left\{\tilde{F}(\beta,\ddot{x},\dot{x},x,t)\right\} \tag{3.9}$$

Only simple matrix multiplication and additions have to be carried out online for calculating the equivalent loads $\tilde{F}(t)$ from measured vibration signal.

## 3.5 Fault Models

The mathematical representation of equivalent loads acting on the damaged system is termed as fault model. Fault models have been developed for prominent faults like unbalance, transverse crack, rotor-stator rub, rotor-bow (Platz et al.,2000). Generally, each fault is represented by a mathematical model describing the relation between the fault parameter $\beta$ and the equivalent force, $F$. Hence $F(\beta, t)$ is a mathematical expression for time history of forces acting on the individual degrees of freedom of the model. The fault vector $\beta$ contains information about the type, position and the magnitude of the fault.

In order to introduce the reference systems used in two-dimensional (2D), finite element model of rotor, consider the two subsequent nodes, the $i^{th}$ and $i+1^{th}$ of an element (Fig. 3.2).
Considering two degrees of freedom for every node, the vector $x^{(i)}$ of generalized displacements of the $i^{th}$ node can be expressed as

$$x^{(i)} = [x_j \quad \theta_{xi}]^T \tag{3.10}$$

$x$ is the generalized displacements of all the nodes of the rotor and is composed of all the ordered vectors $x^{(i)}$

$$x = [x_{i-1} \quad \theta_{xi-1} \quad x_j \quad \theta_{xi} \quad x_{i+1} \quad \theta_{xi+1}]^T \tag{3.11}$$

Therefore, a rotating force $F(\beta, t)$ of amplitude $F^{(k)}$ and rotating moment $\Delta M(\beta, t)$ of amplitude $M^{(k)}$ with frequency $\omega$ acting on the $i^{th}$ node can be represented as

$$F(\beta, t) = [0 \vdots 1 \quad 0 \vdots 0]^T * F^{(k)} \sin \omega t \tag{3.12}$$

Similarly a turning moment can be described by

$$\Delta M(\beta, t) = [0 \vdots 1 \quad 0 \vdots 0]^T * M^{(k)} \sin \omega t \tag{3.13}$$

### 3.5.1 Unbalance Fault Model

The fault model for unbalance (Markert et al., 1999), describes the effect of static and kinetic unbalances at position $i$ of the rotor. A single unbalance $u_i$ is assumed to act at a node position $i$. Then the force at that node is represented as

$$F_{un}(\beta,t) = [1 \quad 0]^{T} u_i \omega^2 \sin \omega t \tag{3.14}$$

The forces at all other nodes are zero. Also let the fault parameter for (which is to be determined) single unbalance be given by

$$\beta_{un} = [I \quad u_i]^{T} \tag{3.15}$$

where $i$ is the node number and $u_i$ is the unbalance.

### 3.5.2 Rub

Rubs generally occur between components of the rotor and stator, consist mostly of harmonics with 1/3,1/2,1 and 2 times the rotor speed. The equivalent forces are therefore approximated by

$$F_{xi} = A_{1/3} \sin\left(\frac{1}{3}\omega t\right) + A_{1/2} \sin\left(\frac{1}{2}\omega t\right) + A_1 \sin(\omega t) + A_2 \sin(2\omega t) \tag{3.16}$$

$$F_{xj} = -\left\{A_{1/3} \sin\left(\frac{1}{3}\omega t\right) + A_{1/2} \sin\left(\frac{1}{2}\omega t\right) + A_1 \sin(\omega t) + A_2 \sin(2\omega t)\right\} \tag{3.17}$$

$$F_{rub}(\beta, t) = [F_{xi} \quad 0]^{T} \tag{3.18}$$

$$F_{j}(\beta, t) = [F_{xj} \quad 0]^{T} \tag{3.19}$$

With the fault vector being described by

$$\beta_{rub} = [i, j, A_{1/3}, A_{1/2}, A_1, A_2] \tag{3.20}$$

The fault vector contains the number of d.o.f in contact as well as the amplitudes $A_n$ of contact force. The contact forces between rotor and stator are opposite in direction.

### 3.5.3. Radial and Angular Misalignment

The finite element model for misalignment has been developed by Bachchmid (2002). The rigid coupling misalignment is simulated by a balanced force system, independent of rotating speed, applied to the coupling flanges. This force system produces a deformation of the beam elements that simulate the coupling, which reproduces the angular and radical deflection of *(i-1)* and *(i+1)* of flanges and makes the rotor assume the static deflection due to this defect.

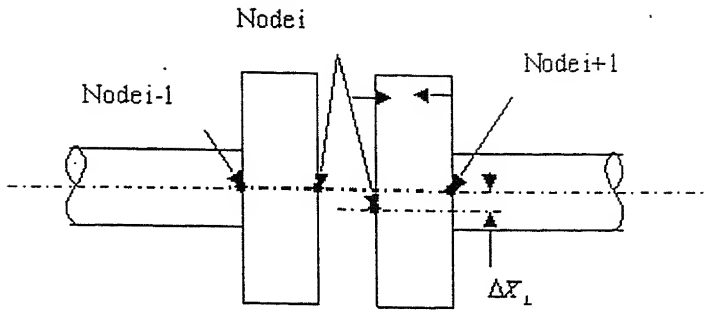


**Fg. 3.3 Representation of radial misalignment between coupling flanges**

Corresponding localization matrix for radial misalignment can be written as (Fig.3.3)

$$F_{rm}(\beta, t) = [K_x \; K_{\theta,i}]^T \begin{bmatrix} 1 \\ 0 \end{bmatrix} \begin{bmatrix} \Delta X_L Sin\omega t \\ 0 \end{bmatrix} \tag{3.21}$$

with the fault vector

$$\beta_{rm} = [I \;\; \Delta X_L]^T \tag{3.22}$$

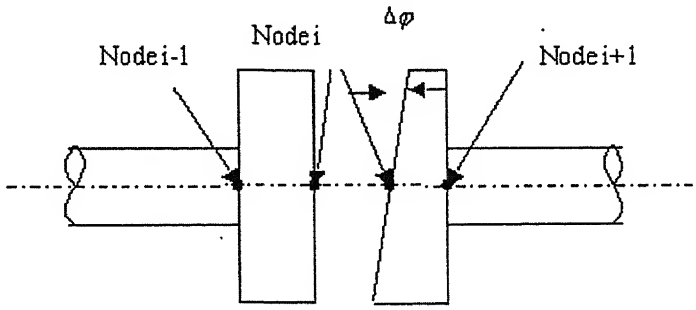


**Fig.3.4. Representation of the angular misalignment of two flanges of coupling**

Localization matrix for angular misalignment can be written as (Fig.3.4)

$$F_{am}(\beta, t) = [K_x \; K_{\theta,i}]^T \begin{bmatrix} 0 \\ 1 \end{bmatrix} \begin{bmatrix} 0 \\ \Delta\varphi Cos\varpi t \end{bmatrix} \tag{3.23}$$

with the fault vector

$$\beta_{am} = [I \;\; \Delta\varphi]^T \tag{3.24}$$

## 3.6 Time Domain Least Square Fitting

A least square algorithm is used to achieve the best fit between the measured equivalent forces $\tilde{F}_i(t)$ and theoretical ones $F_i(\beta,t)$ produced by the fault models by adjusting the fault parameters $\beta_i$ for all faults taken into account. The procedure is described by the following equation

$$\left|\sum_i F_i(\beta_i,t)-\tilde{F}(t)\right|^2 dt = \min \tag{3.25}$$

Starting with an initial guess, the least squares algorithm varies the fault parameters $\beta_i$ of each fault model until the deviation is minimal.

## 3.7 Remarks

The identification procedure can be represented in the form of a flow-chart as shown in Fig. 3.5.

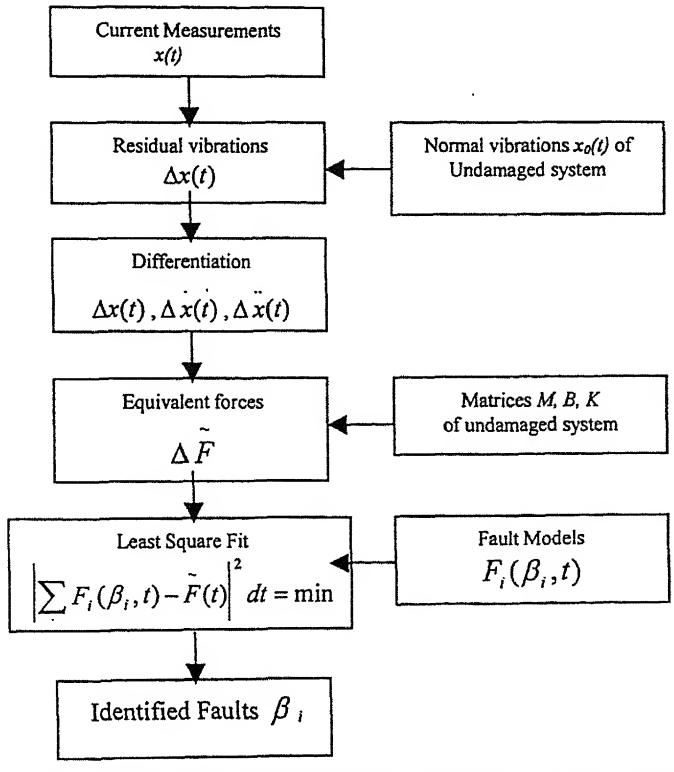


**Fig. 3.5 Flow chart of the identification procedure**

The implementation of the procedure on a test rotor-bearing system is discussed in the subsequent chapters.

# CHAPTER 4

# EXPERIMENTAL INVESTIGATIONS

Experimentation is carried out on a specially designed rig called the Machinery Fault Simulator (MFS). The MFS is the comprehensive machine for simulating, studying and learning vibration signatures of machinery defects. The rig is connected to data acquisition system through proper instrumentation. Accelerometers and proximity pick-ups are used for picking up the vibration signals from various stations. Data is acquired and processed by Virtual Instrumentation techniques of LabVIEW software. After collecting the vibration signals and extracting features the vector is fed to FEM model is embedded into the LabVIEW software. This integrates the entire process of acquiring the data, processing of data and testing for fault diagnosis into a single package.

## 4.1 Experimental Test Rig

The Machinery Fault Simulator (Fig. 4.1) is a desktop rotor model, which consists of a shaft supported in two roller bearings and driven by a DC motor. A flexible coupling is used to compensate for any misalignment between the bearings and motor, as well to prevent any unwanted dynamic effects occurring in the motor being transmitted through the coupling into the rotor itself. Discs can be mounted on the shaft at desired locations. There is provision for connecting a gearbox through a belt drive consisting of two V-belts. The kit also carries a reciprocating mechanism, which can in turn be connected through the gearbox. The rig has an adjustable speed range of 0 - 6000 rpm (0-100 Hz). Different loading conditions can be simulated in MFS by setting torque in an adjustable torque magnetic brake. The kit also carries a rubbing mechanism, which can be used for simulate the rub.

## 4.2 Instrumentation

During the present study, five sensors were used to pick up the vibration signals at the following locations (Fig 4.2, 4.3). The sensors and locations are described in the following:

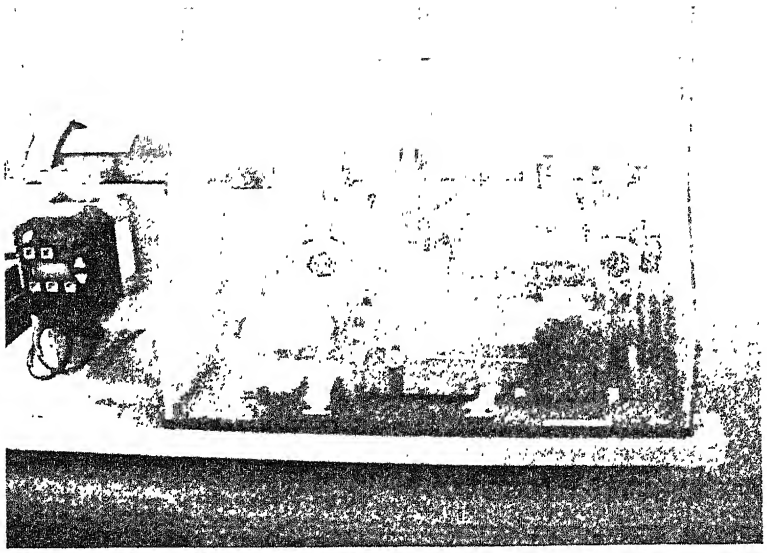

**Fig. 4.1 Machinery fault simulator**

**Fig. 4.2 Instrumentation and data acquisition**

(i) Bearing housing vibration, in the vertical direction at the left side bearing: Sensor - accelerometer (model 4374, Bruel and Kjaer make) along with a charge amplifier, (model 2635, of the same make).

(ii) Shaft displacement in the vertical direction at near the left disk: Sensor - non-contact type eddy current displacement probes (Proximitor), model 3300 RAM, Bentley Nevada make; associated transducer and TK 15 signal conditioner.

(iii) Shaft displacement in the vertical direction at middle of the shaft: Sensor - same configuration as in (ii) above.

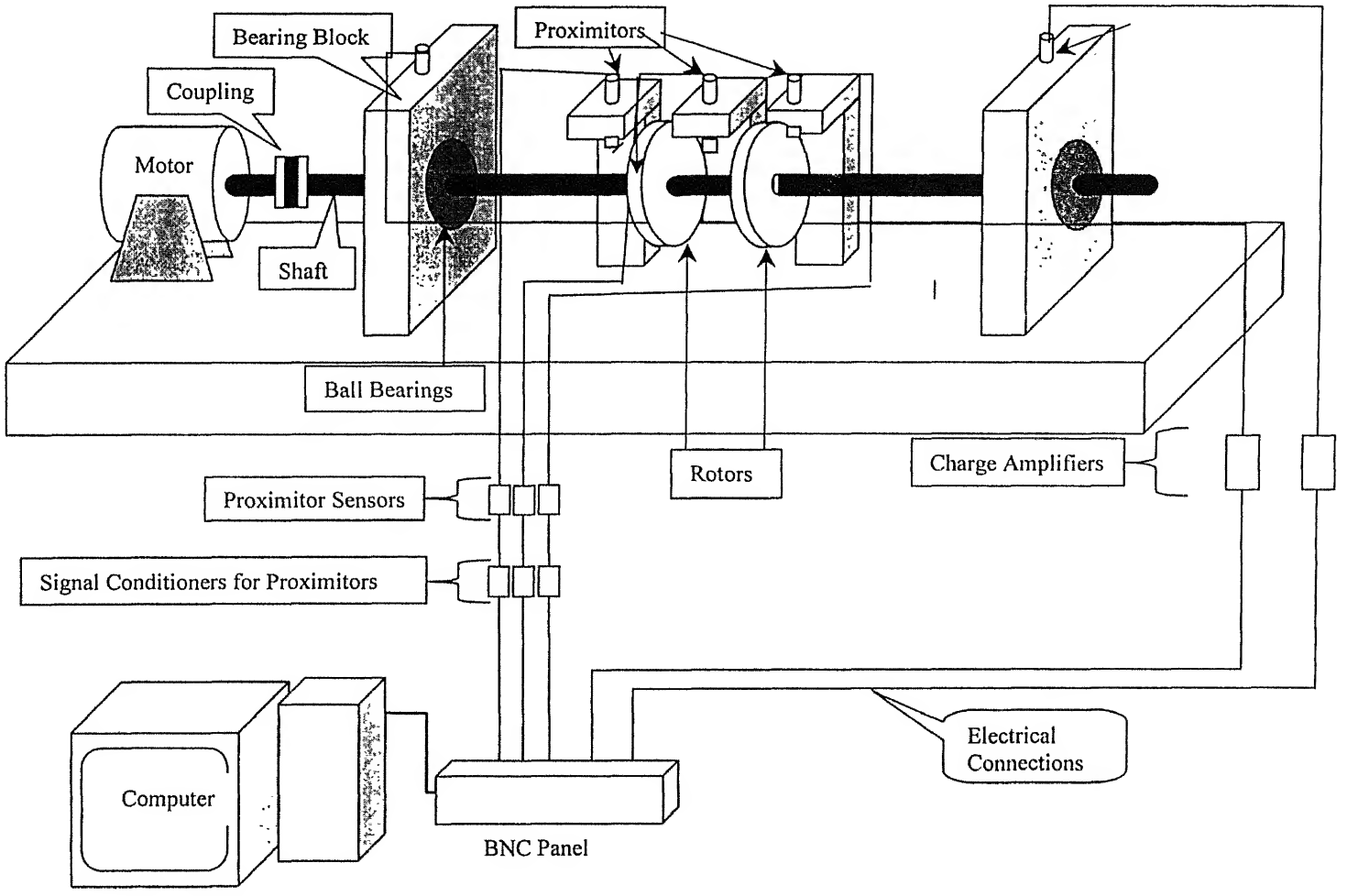


**Fig4.3 schematic diagram of the experimental set up and Instrumentation**

(iv) Shaft displacement in the vertical direction at near the right disk: Sensor - same configuration as in (ii) above.

(v) Bearing housing vibration, in the vertical direction at the right side bearing: Sensor - accelerometer (model 4374, Bruel and Kjaer make) along with a charge amplifier, (model 2635, of the same make).

Vibration data is obtained simultaneously from the above five stations and is acquired into a P-4 computer using a Data Acquisition Card (PCI-6024E, National Instruments, Texas, 200K samples per second, 12 bit, 16 analog inputs) and LabVIEW software. LabVIEW is a graphical programming language, unlike C or BASIC, which are text base language. The program of LabVIEW is called virtual instrument because its appearance, and its operation that can imitate actual instruments. On the front panel of the program one sees the graphs, icons, knobs etc like actual instruments but one can control them programmatically. LabVIEW is a data flow programming language in which a node executes only when it has all its inputs. It is a general-purpose programming system and includes various tools for data acquisition, data analysis, data presentation, and storage. An interactive user interface of a VI, called *front panel* is used to pass on user-defined parameters into the program, called *block diagram* and program's output parameters are displayed in the front panel. Since user interactive programs can be written for various applications and output parameters of the program can be displayed in text as well as graphical form, it offers tremendous potential for developing wide variety of applications. The front panel is used for data input in form of text box, knobs, buttons etc. and output in the form of text box, figure box, graphs, plots etc. Modular programming techniques make LabVIEW suitable for simulating a large number of instruments limited only by the data acquisition card used.

## 4.3 Data Acquisition, Storage and Display

For data acquisition, data storage and display a virtual instrument is made using LabVIEW. This program has following features:

(a) Time domain vibration data acquisition and display from five channels with following user controls (figures/text within brackets indicate default values):

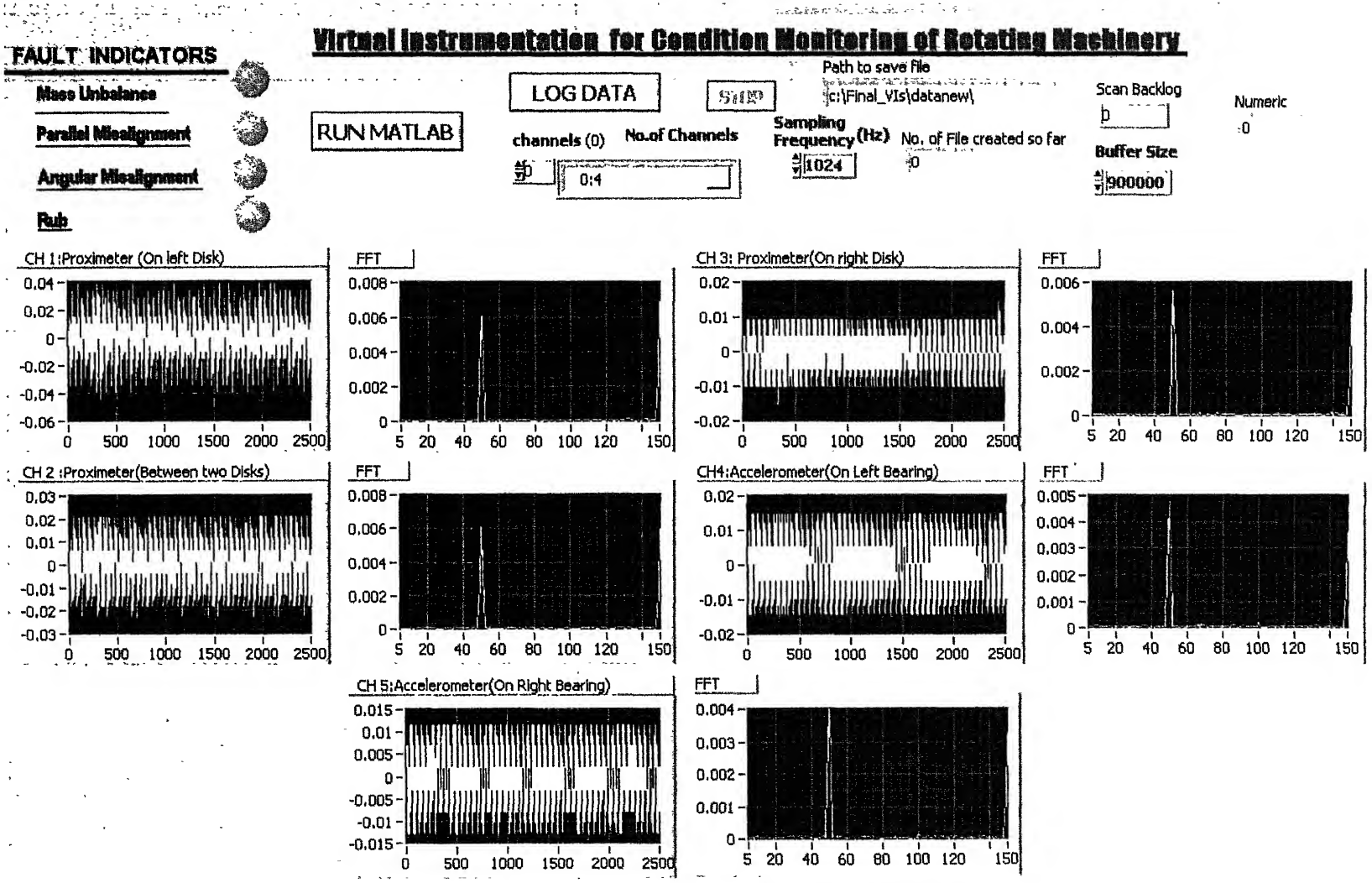


**Fig 4.4(a) Front panel of data acquisition VI**

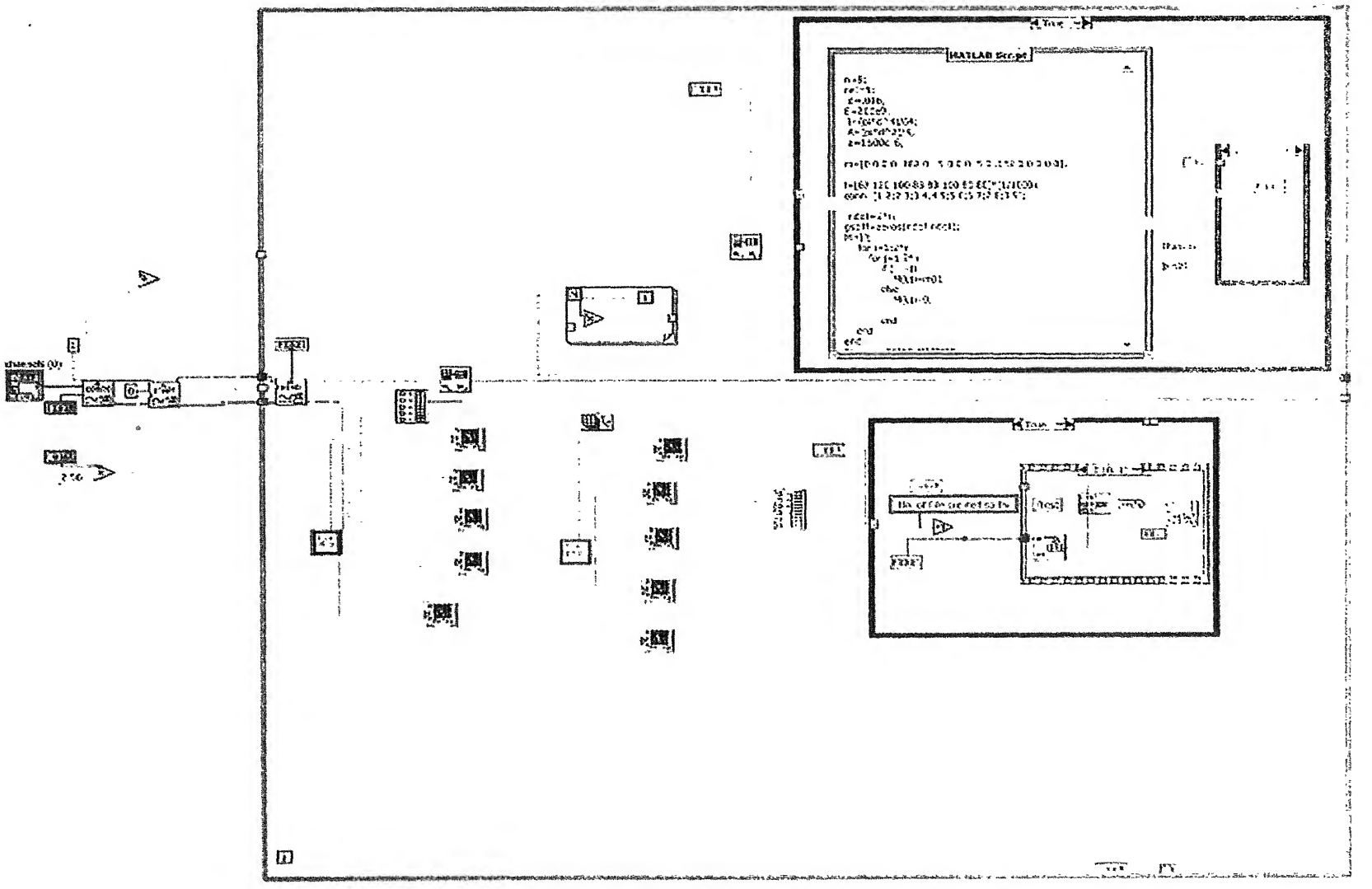

**Fig.4.4(b) Block diagram of VI**

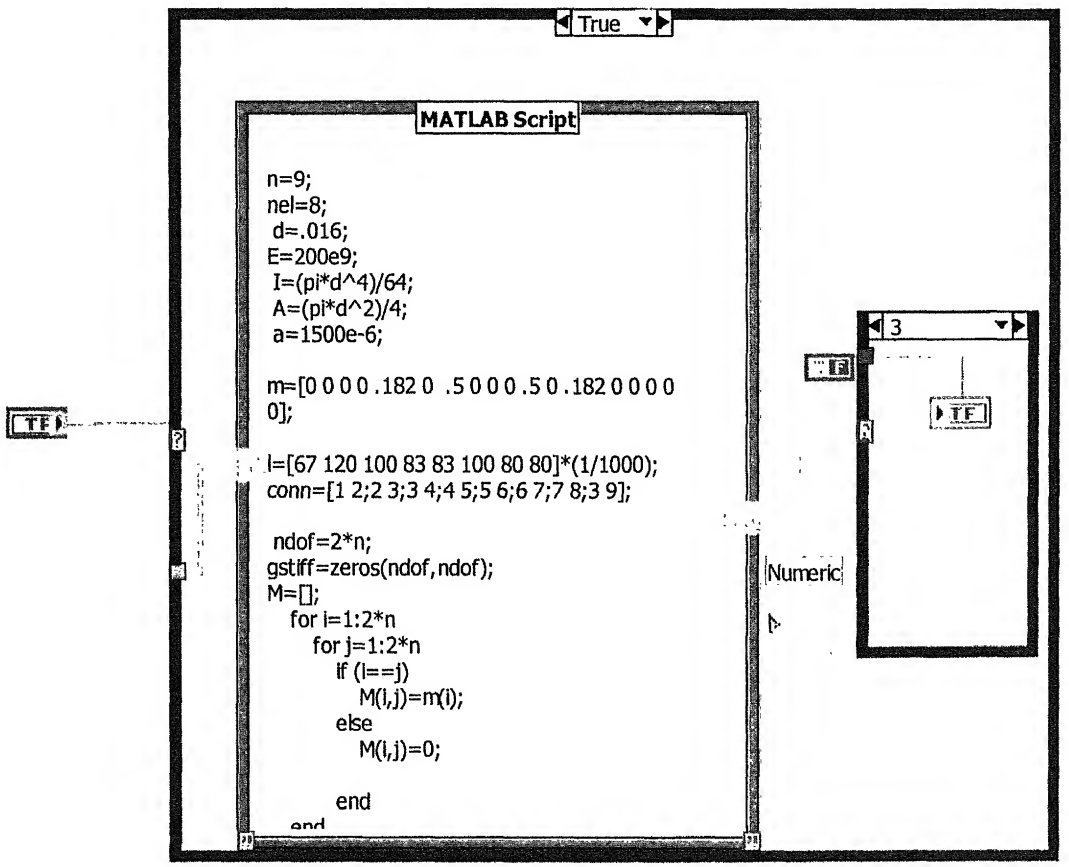


**Fig 4.5 Fem model of rotor segment VI**

(i) Scan Rate (2621)

(ii) Number of data points to be read before display (4096).

(iii) Device and Channel numbers from which to acquire data (Device No. 1 and Channel Nos. 0 to 4).

(b) A Hanning window is then applied to the acquired time domain signal. Fast Fourier Transform (FFT) of the time signal is carried out and the FFT is displayed in 'real' time along with the time domain signal on the front panel. Provision is also given on the front panel for the user to select the desired frequency range for FFT display.

(c) Option for logging the time domain data and frequency domain data into the hard disc at any desired instant of time.

(d) Run *FE model and Diagnose* control for online testing of the faults in the rotor.

(e) The *output of the FE model*, which is indicative of the *fault* predicted. Circular Indicators, one for each type of fault, are provided on the Front Panel, which are *GREEN* in colour in absence of any fault. If a particular fault occurs the indicator pertaining to the fault turns *RED*.

Fig 4.4 shows the Front Panel of the VI. The Block Diagram of the VI is given in Fig 4.4(a)

## 4.4 Fault Simulation

The list of various faults, which were introduced for this study, is given below:

(i) Mass unbalance on right rotor

(ii) Parallel Misalignment

(iii) Angular Misalignment

(iv) Rub

Six sets of vibration signals were acquired for each of the above four separate faults. Each set includes signals from the five sensors mentioned earlier. Time domain vibration signals were acquired at a scan rate of 2621 samples/sec. Frequency domain transformation was carried out on line using an FFT algorithm available in LabVIEW.

While standard procedures were available for introduction of faults (i) – (iii), on the Machinery Fault Simulator, a special Rubbing Kit was designed, instrumented and then calibrated to carry out the investigations on the rubbing phenomenon.

The set up for rub is shown in Fig. 4.5(a). The kit in assembled state is shown in Fig. 4.5(b). It consists of an annular tube containing a rubber insert. The rubber insert is pressed on the rotating shaft to cause rub. The force exerted by the insert is measured by a piezoelectric crystal, which was sandwiched inside the annular tube. The sensor was calibrated by subjecting the rubber insert to known amount of forces and noting down the corresponding voltage signal produced by the sensor. The individual components of the Rub Kit are shown in Fig. 4.5(c).

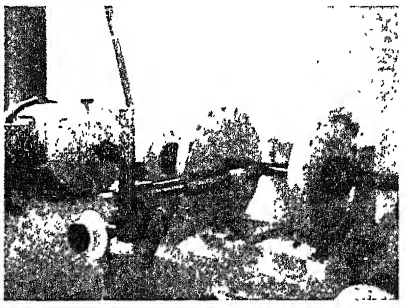

**Fig.4.5(a) Rubbing setup**

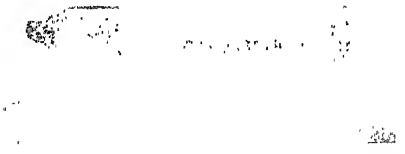

**Fig 4.5(b) Rubbing kit assembly**

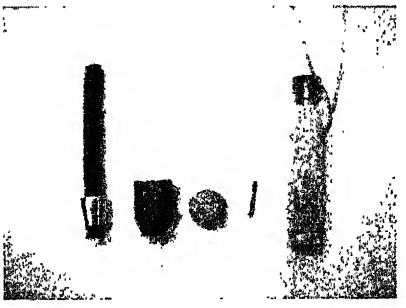

**Fig 4.5(c) Individual components of rubbing kit**

Typical time domain data and FFT, obtained from three proximity sensors and two accelerometers for some faults, are shown in Figs.4.6 - 4.10

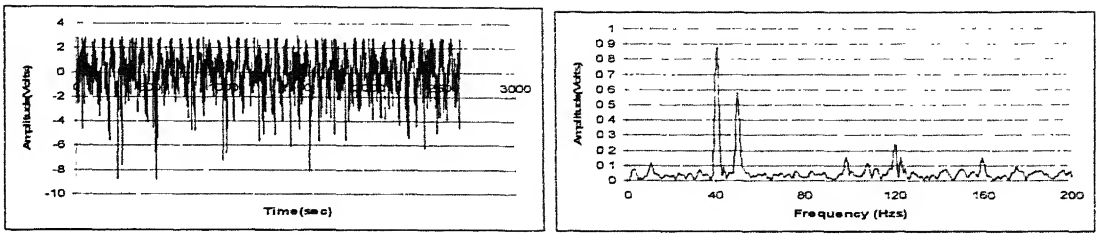


(a) Left proximeter

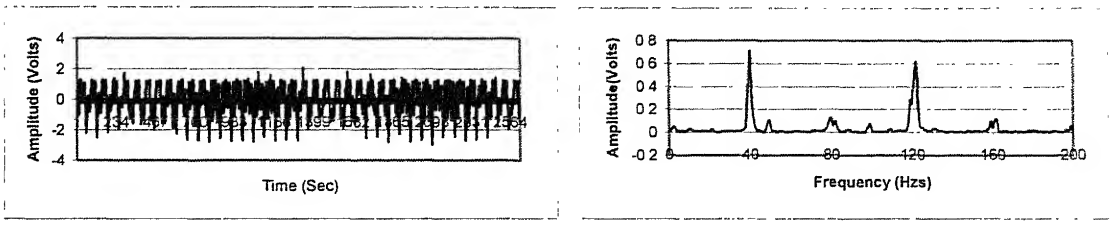


(b) Middle proximeter

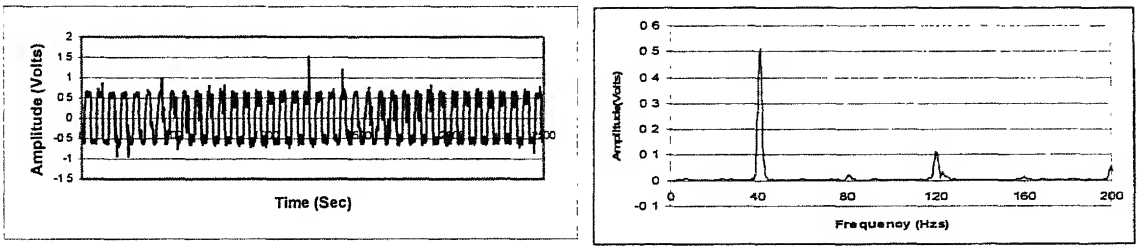


(c) Right proximeter

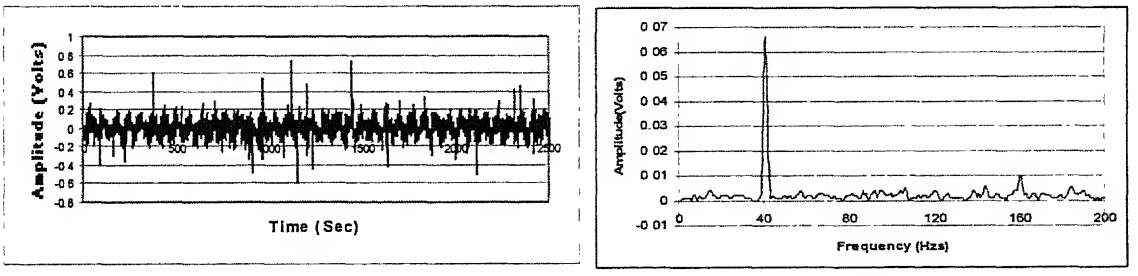


(d) Left accelerometer

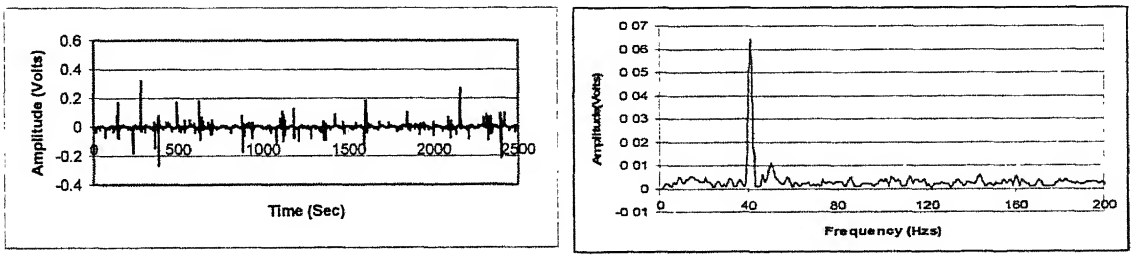


(e) Right accelerometer

**Fig 4.6 Time and frequency domain signals for undamaged system**

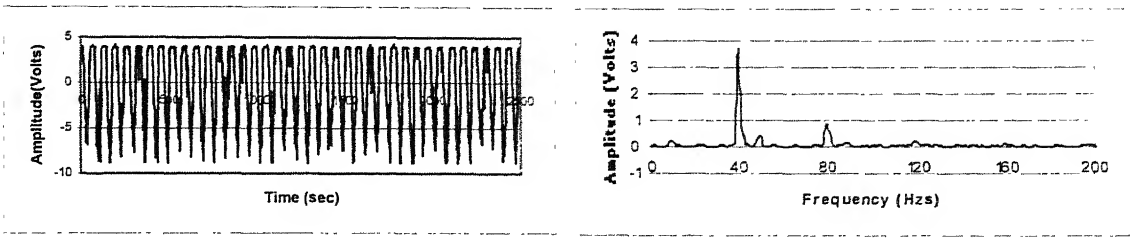


(a) Left proximeter

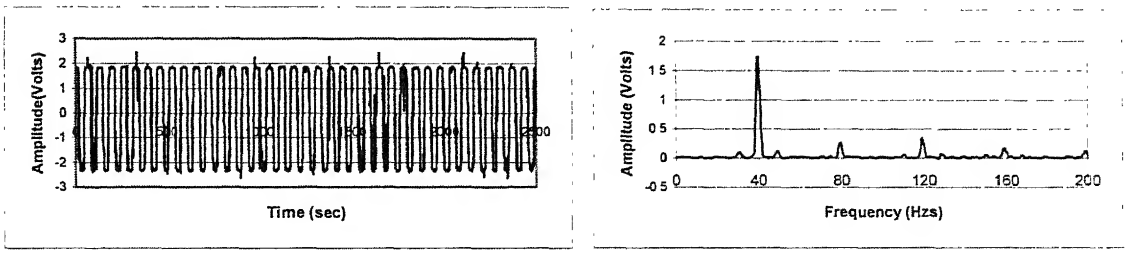


(b) Middle proximeter

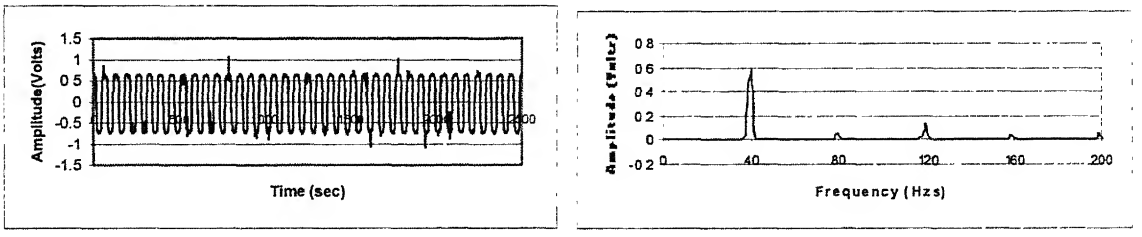


(c) Right proximeter

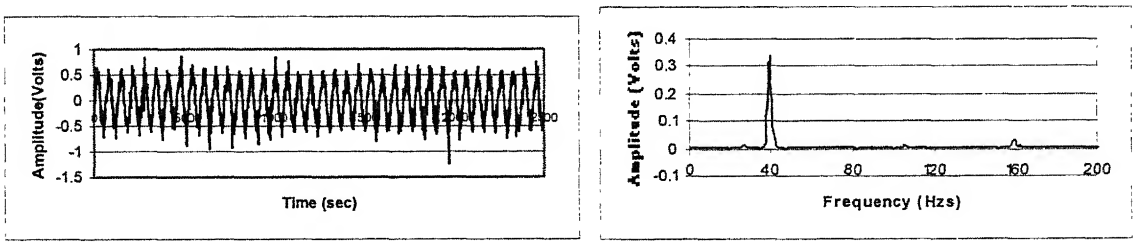


(d) Left accelerometer

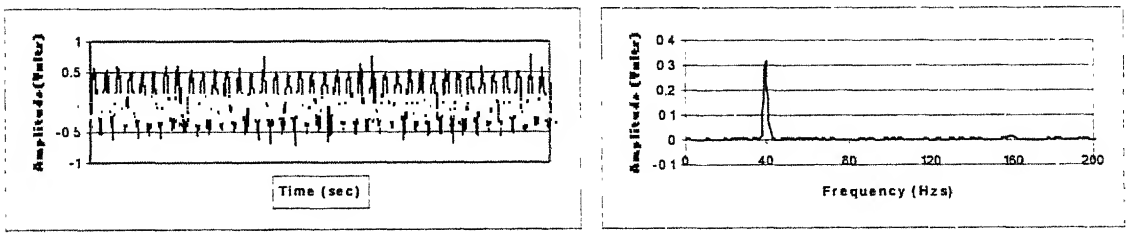


(e) Right accelerometer

Fig 4.7 Time and frequency domain signals for unbalance

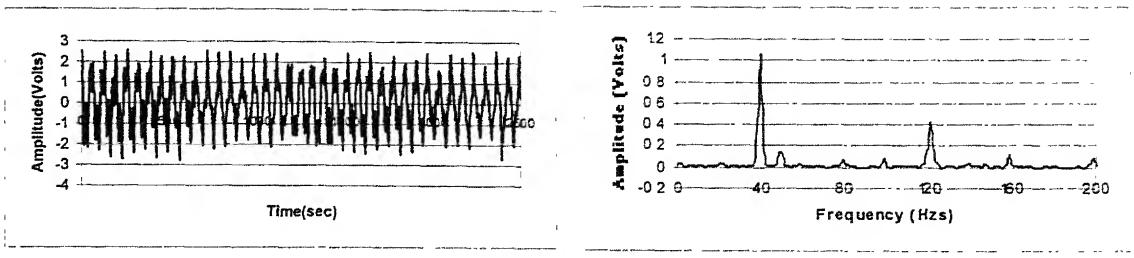


(a)Left proximeter

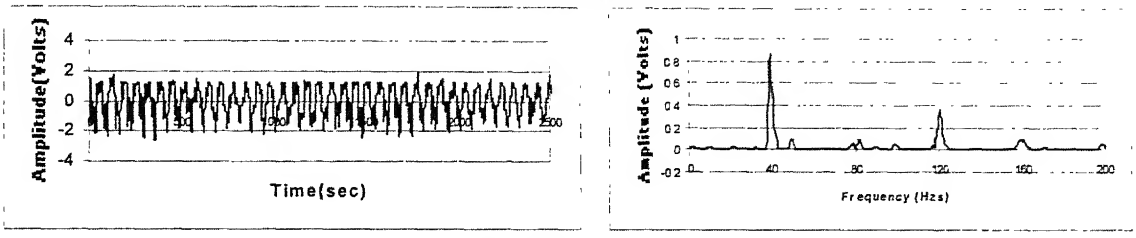


(b) Middle proximeter

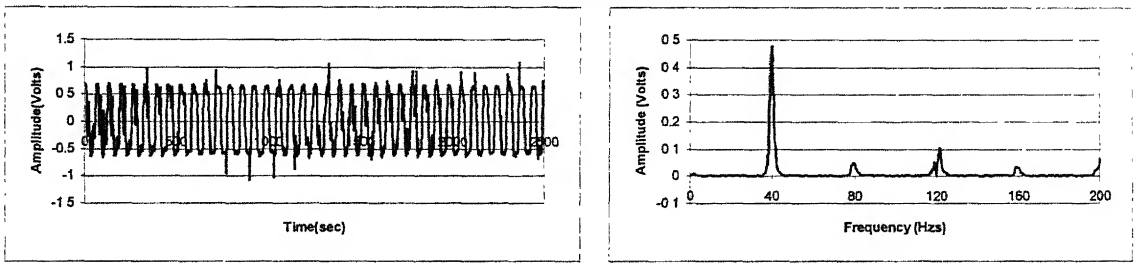


(c) Right proximeter

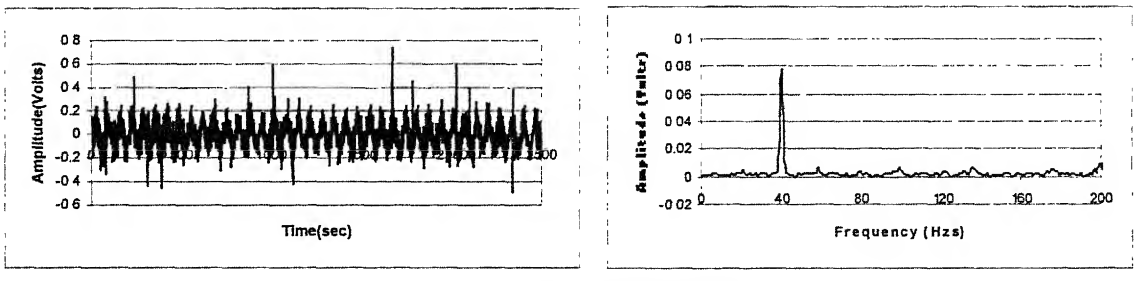


(d) Left accelerometer

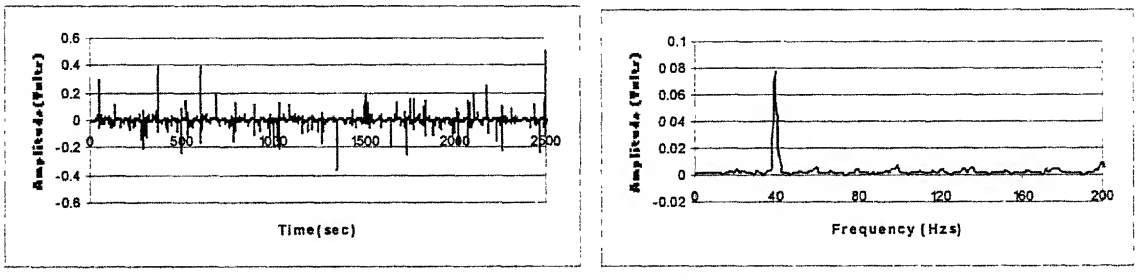


(i) Right accelerometer

**Fig 4.8 Time and frequency domain signals for radial misalignment**

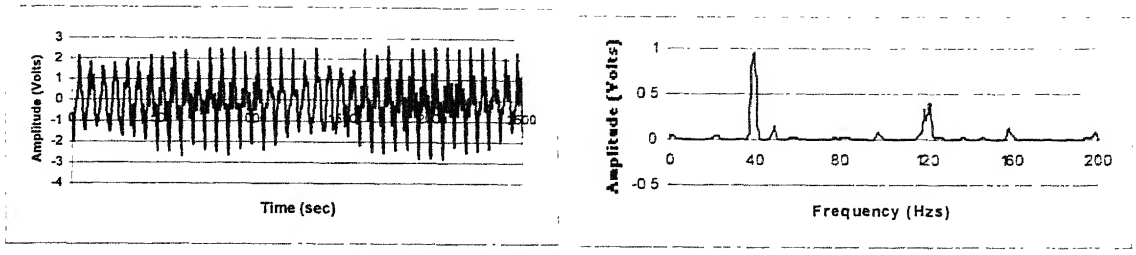


(a)Left proximeter

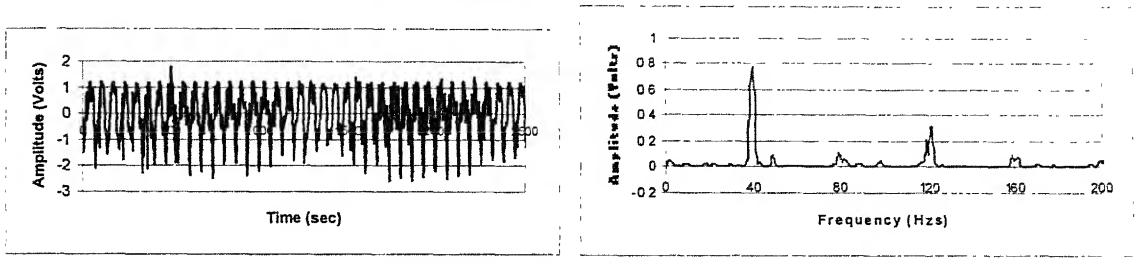


(b) Middle proximeter

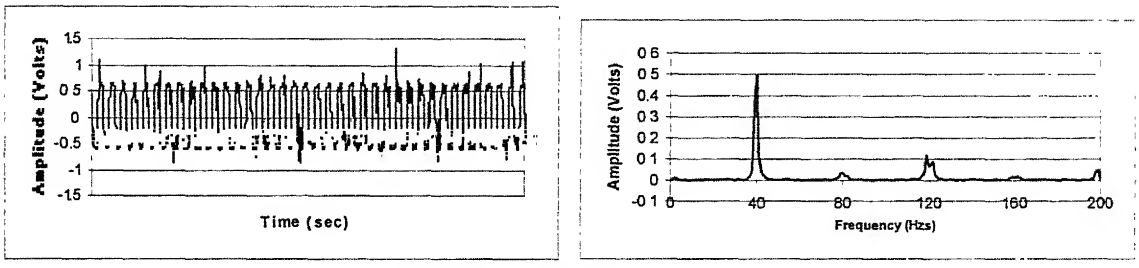


(c) Right proximeter

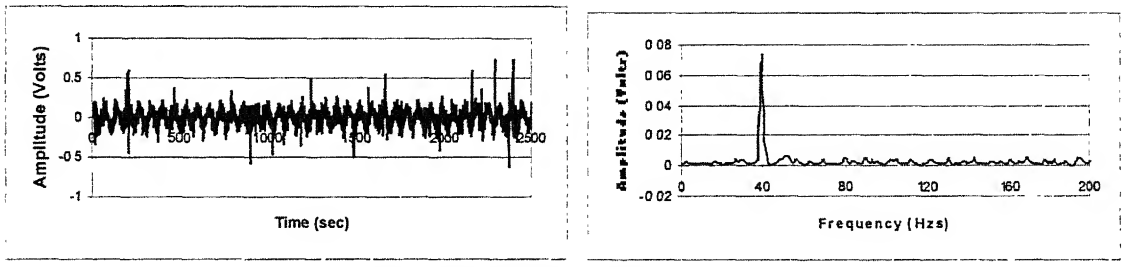


(d) Left accelerometer

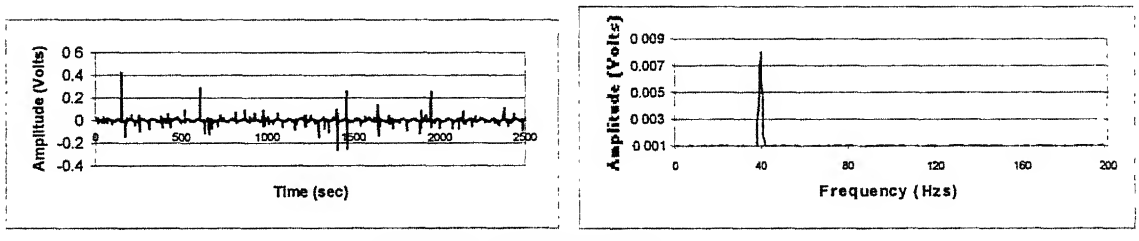


(e) Right accelerometer

**Fig 4.9 Time and frequency domain signals for angular misalignment**

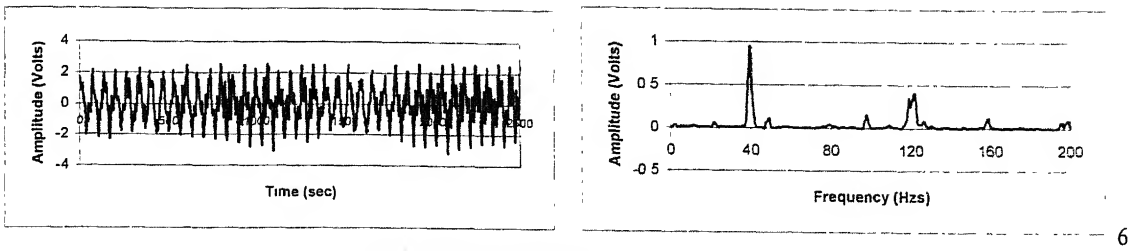


6

(a)Left proximeter

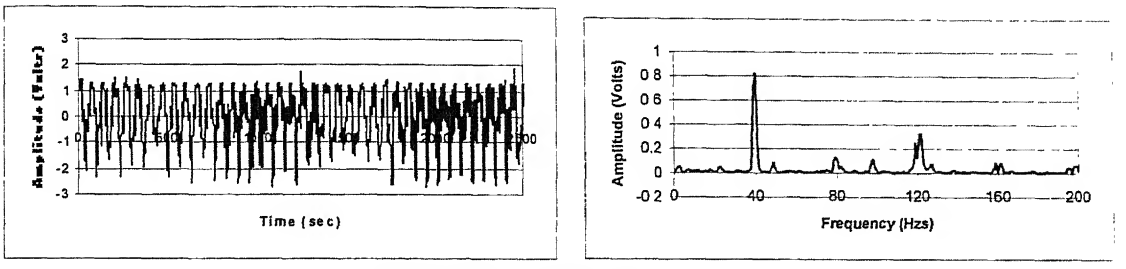


(b) Middle proximeter

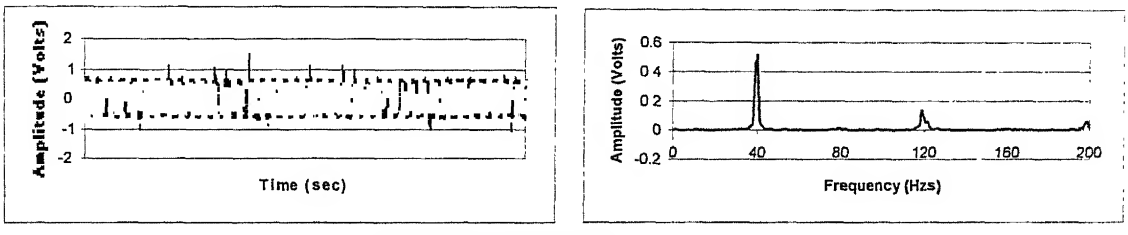


(c) Right proximeter

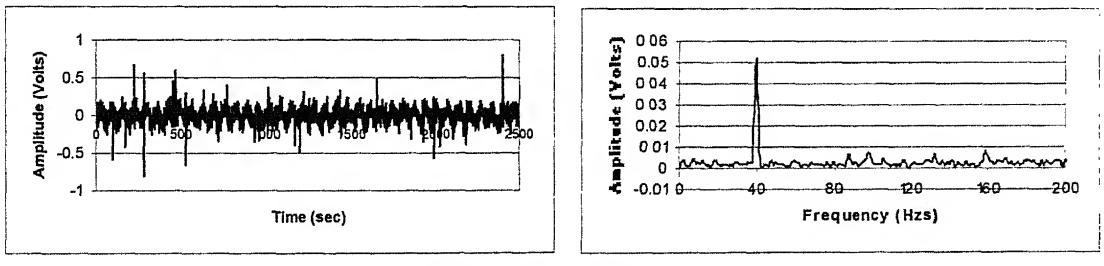


(d) Left accelerometer

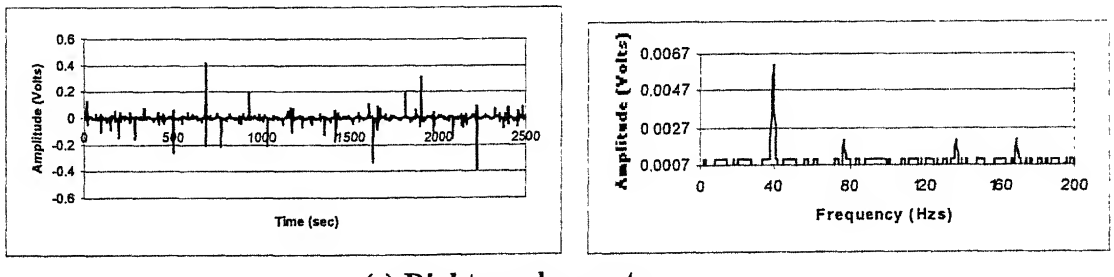


(e) Right accelerometer

**Fig 4.10 Time and frequency domain signals for rub**

# CHAPTER 5

# RESULTS AND DISCUSSIONS

As described earlier for the present work four faults were introduced in the test rig. Normal condition vibrations are recorded at a rotor speed of 2400 rpm (40 Hz) at five sensor locations. For the faults under consideration the time domain and the frequency domain data was acquired and the digital data is stored in separate files. For each fault a set of six signals was recorded, and averaged for further analysis.

## 5.1 Amplitude Extraction

Attempt has been made here to integrate the Feature Extraction and Analysis with the Data Acquisition process described in the earlier chapter. On line data acquisition is carried out by developing codes in LabVIEW. Feature extraction and analysis codes are written in MATLAB and embedded in the LabVIEW codes to construct a unified fault detection package.

The basic step is to obtain amplitude information. An algorithm has been developed for automatic extraction of running frequency and amplitude from the time domain data. This algorithm is employed for obtaining the values of $x_0(t)$ and $x(t)$, discussed in Chapter 3. The algorithm takes the frequency domain spectrum as input and provides the amplitude at the rotor running frequency and its harmonics.

The algorithm is written in MATLAB and follows the following steps:

(1) The first column of FFT data stored in the file contains frequency information. As a first step the absolute values of differences of all values of frequency with the running frequency are calculated and stored in an array.

(2) The minimum of the array gives the index of the running frequency.

(3) Three previous and three latter values at that index in all channels is stored separately.

(4) The maximum of above seven values for each channel is taken as the amplitude of vibration at running speed.

The algorithm for amplitude extraction is shown in Fig.5.1

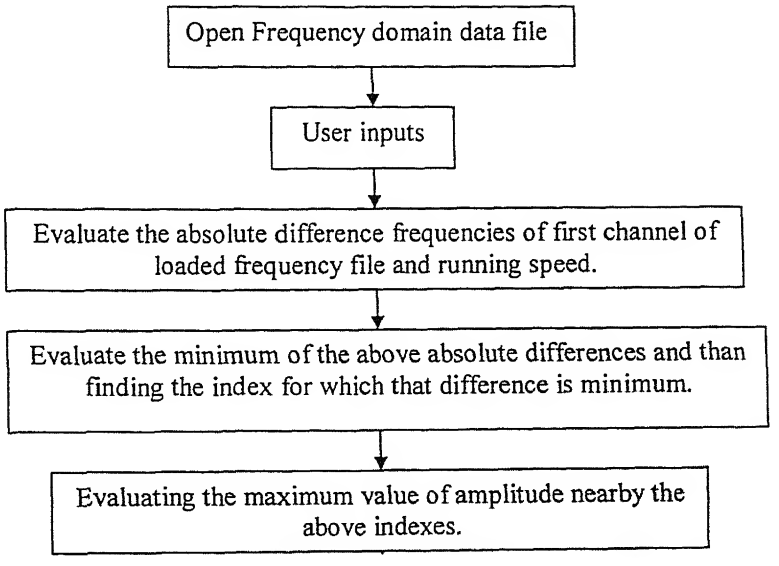


**Fig. 5.1 Algorithm for amplitude extraction at running frequency.**

The program has the following user interactive controls:

(i) Rotational Speed of the machine

(ii) The width of the frequency band on either side of the rotational speed.

Further processing of FFT signals for damaged and undamaged system, recorded in files, is carried out by computing the averages at the running frequency to obtain values of the normal vibration $x_0(t)$ and damaged system vibration $x(t)$.

Typical $x_0(t)$ values and $x(t)$ values thus obtained for various faults are given in Table 5.1. The values in this table correspond to the measurements taken with five sensors, which included three proximity pick-ups and two accelerometers.

**Table 5.1 Typical amplitude data (volts)**

| Sensor location | No-fault data $x_0(t)$ | Mass Unbalance $x(t)$ | Radial misalignment $x(t)$ | Angular misalignment $x(t)$ | Rub $x(t)$ |
|---|---|---|---|---|---|
| Left proximeter | 0.800 | 3.7090 | 1.0320 | 0.9500 | 0.9500 |
| Middle proximeter | 0.680 | 1.7180 | 0.8790 | 0.7710 | 0.7850 |
| Right proximeter | 0.506 | 0.5750 | 0.4820 | 0.4860 | 0.5160 |
| Left accelerometer | 0.066 | 0.3360 | 0.0800 | 0.0720 | 0.0490 |
| Right accelerometer | 0.064 | 0.3160 | 0.0010 | 0.0080 | 0.0050 |

Residual vibration, $\Delta x(t)$, is then obtained and the equivalent force vector $\tilde{F}(t)$ for the fault is computed in accordance with equations 3.2.

The rotations $\theta$ at various nodes are computed using the simple trigonometric formula $\tan\theta = (x_i - x_{i-1})/L$, where $x_i$ and $x_{i-1}$ are the measured displacements at two consecutive nodes and $L$ is the element length. Typical values of residual displacements from experimental data are shown in Fig 5.2. The horizontal axis on these plots shows the degrees of freedom considered in the FE model (9 nodes x 2 degrees of freedom, $x$ and $\theta$).

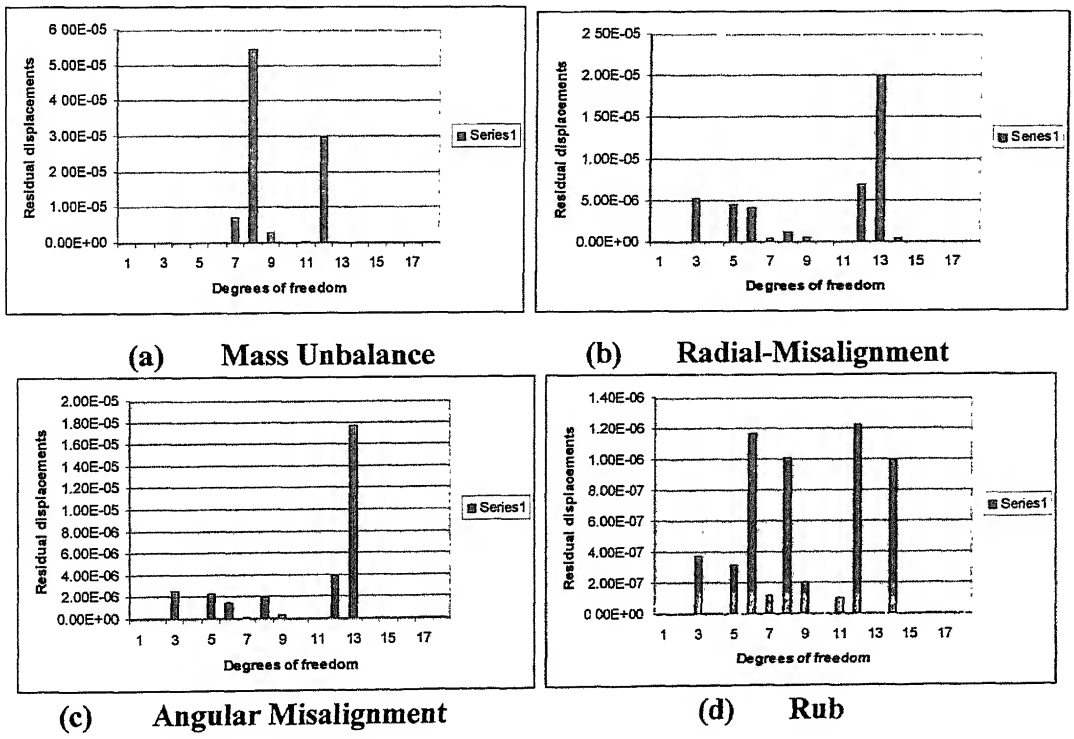


(a) Mass Unbalance (b) Radial-Misalignment

(c) Angular Misalignment (d) Rub

**Fig 5.2 Residual Vibrations $\Delta x(t)$ for Various Faults**

Residual acceleration vector $\Delta x(t)$ is found by differentiating the residual displacement vector ( $\Delta x(t)$ . Typical residual vibration $\Delta x(t)$ vectors for four faults are shown in Fig 5.3.

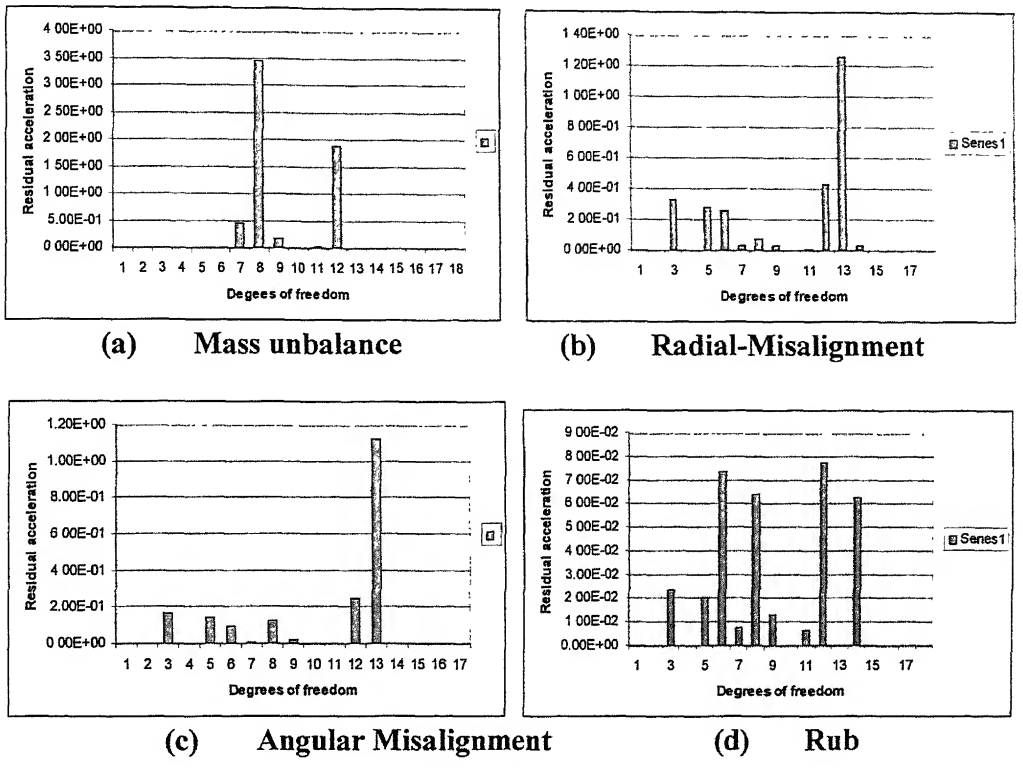


(a) Mass unbalance (b) Radial-Misalignment

(c) Angular Misalignment (d) Rub

**Fig. 5.3 Residual Accelerations $\Delta \ddot{x}(t)$ for Various Faults**

## 5.2 Experimental Force Vector ( $\tilde{F}(t)$ )

The mass and stiffness matrices [$M$] and [$K$] are estimated using equations 3.5-3.8 and the equivalent force vector $\tilde{F}$ is calculated using equation 3.9. Typical Experimental force vector ( $\tilde{F}(t)$ ) for four faults are shown in Table 5.3.

Table 5.2 Experimental force vectors (Newtons)

| Degrees of freedom | Mass Unbalance $(\tilde{F}_{un}(t))/\mathrm{Sin}\,\omega t$ | Radial misalignment $(\tilde{F}_{rm}(t))/\mathrm{Sin}\,\omega t$ | Angular misalignment $(\tilde{F}_{am}(t))/\mathrm{Sin}\,\omega t$ | Rub $(\tilde{F}_{rub}(t))$ |
|---|---|---|---|---|
| 1 | 0.00 | 0.00 | 0.00 | 0.00 |
| 2 | 0.00 | 0.00 | 0.00 | 0.00 |
| 3 | 0.00 | 137.41 | -2.11 | 1.01 |
| 4 | 0.00 | -4.21 | 68.54 | -0.29 |
| 5 | -76.54 | -2.43 | -1.22 | -0.173 |
| 6 | -3.48 | 1.96 | 9.91 | -0.16 |
| 7 | 106.86 | -33.61 | -1.83 | -0.10 |
| 8 | -3.33 | 1.61 | 8.36 | -2.94 |
| 9 | -13.91 | 4.44 | 3.24 | 0.64 |
| 10 | 2.62 | 0.18 | 6.17 | -0.78 |
| 11 | -26.93 | 14.70 | 1.33 | 0.001 |
| 12 | -0.24 | 7.60 | 6.78 | 0.09 |
| 13 | 10.21 | 1.10 | 9.74 | -0.003 |
| 14 | -0.32 | 7.58 | 6.77 | 0.125 |
| 15 | 0.00 | 0.00 | 0.00 | 0.00 |
| 16 | 0.00 | 0.00 | 0.00 | 0.00 |
| 17 | 0.00 | 0.00 | 0.00 | 0.00 |
| 18 | 0.00 | 0.00 | 0.00 | 0.00 |

## 5.3 Model Force Vectors

The Model force vectors computed through FE technique vectors are calculated by substituting equivalent forces and moments in equations (3.16, 3.19, 3.24, and 3.26) referred in Chapter 3. These force vectors for various faults are given in Table 5.3

Table 5.3 FEM force vectors (Newtons)

| Degrees of freedom | Mass Unbalance ($F_{un}(t)$) | Radial misalignment ($F_{rm}(t)$) | Angular misalignment ($F_{am}(t)$) | Rub ($F_{rub}(t)$) |
|---|---|---|---|---|
| 1 | 0 | 0 | 0 | 0 |
| 2 | 0 | 0 | 0 | 0 |
| 3 | 0 | 191.37*Sin $\omega t$ | 0 | 0 |
| 4 | 0 | 0 | 70.63*Cos $\omega t$ | 0 |
| 5 | 0 | 0 | 0 | 0 |
| 6 | 0 | 0 | 0 | 0 |
| 7 | 95.12*Sin $\omega t$ | 0 | 0 | 0 |
| 8 | 0 | 0 | 0 | 0 |
| 9 | 0 | 0 | 0 | 1.75 |
| 10 | 0 | 0 | 0 | 0 |
| 11 | 0 | 0 | 0 | 0 |
| 12 | 0 | 0 | 0 | 0 |
| 13 | 0 | 0 | 0 | 0 |
| 14 | 0 | 0 | 0 | 0 |
| 15 | 0 | 0 | 0 | 0 |
| 16 | 0 | 0 | 0 | 0 |
| 17 | 0 | 0 | 0 | 0 |
| 18 | 0 | 0 | 0 | 0 |

## 5.4 Unbalance Identification

A residual unbalance of 14.76 x $10^{-4}$ kg m was applied on left disk (node 4). Referring to the fault model for unbalance, given in Chapter 3 (equations 3.14), the fault vector is described by $\beta_{un} = [i \quad u_i]^T$. The force computed from the FE model is depicted in Fig 5.4(a). The equivalent force computed from experimental data is shown in Fig. 5.4 (b).

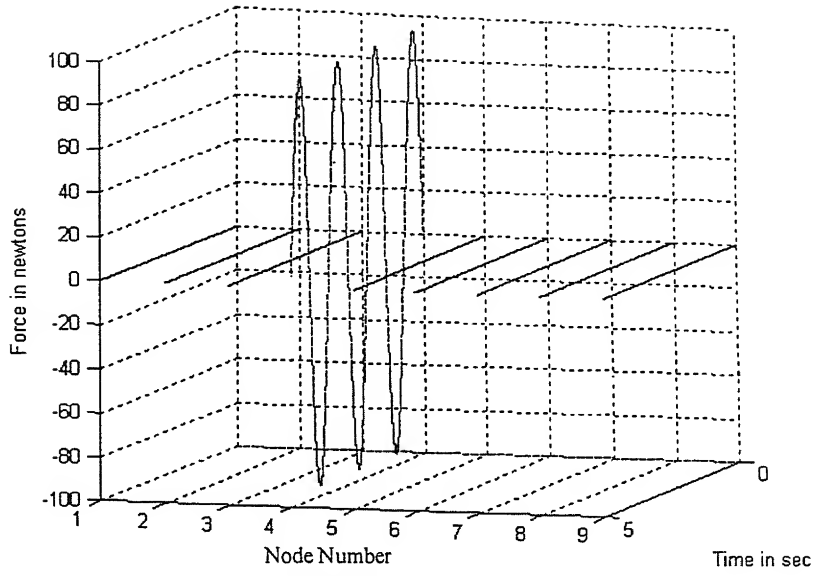


**Fig 5.4(a) FE Model based equivalent forces**

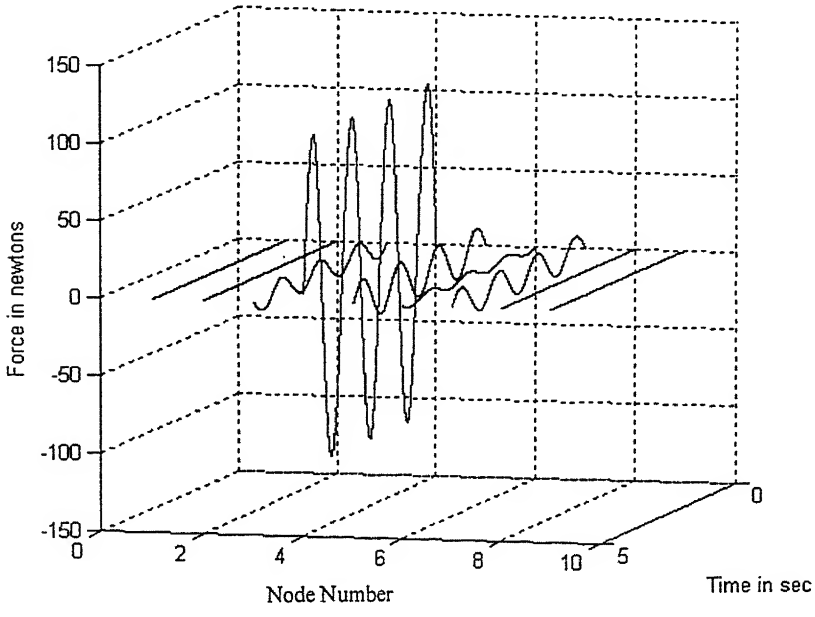


**Fig 5.4(b) Equivalent forces from experimental data**

Close resemblance between the two plots is indicative of the efficiency of the adopted approach for fault identification. The summary of these observations is given in Table 5.4.

Table 5.4 Summary of diagnosis for Unbalance

| Applied unbalance $(u_i)10^{-4}$(kg-m) | Identified unbalance $(u_i)10^{-4}$(kg-m) | Location of applied unbalance (i) | Identified Location of fault (i) |
|---|---|---|---|
| 14.76 | 16.83 | 4 | 4 |

## 5.5 Radial Misalignment Identification

A parallel misalignment 0.653 mm is introduced on coupling (node 2) for simulation of Radial Misalignment. Referring to the fault model for radial misalignment given in Chapter 3 (equation 3.21), the fault vector is described by $\beta_{rm} = [i \quad \Delta X_L]^T$. The force computed from the FE model is depicted in Fig 5.5(a). The equivalent force computed from experimental data is shown in Fig. 5.5 (b).

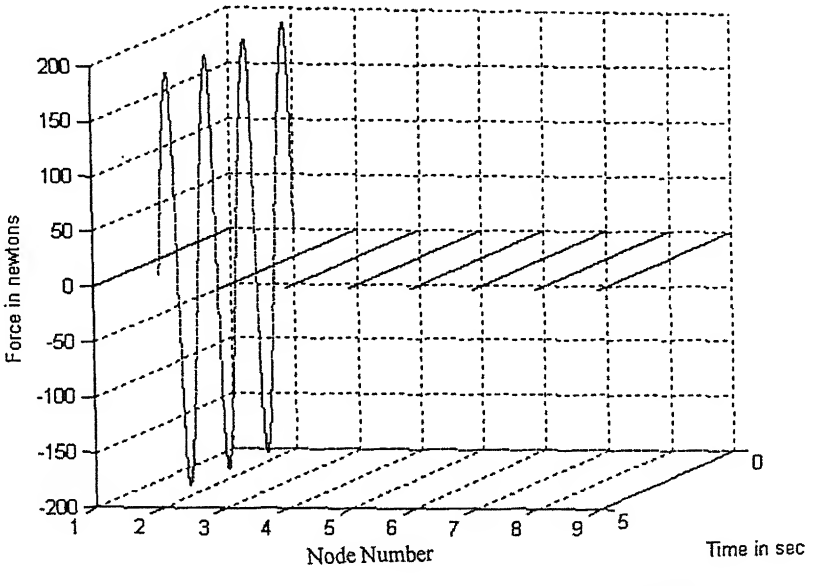


**Fig 5.5(a) FE Model based equivalent forces**

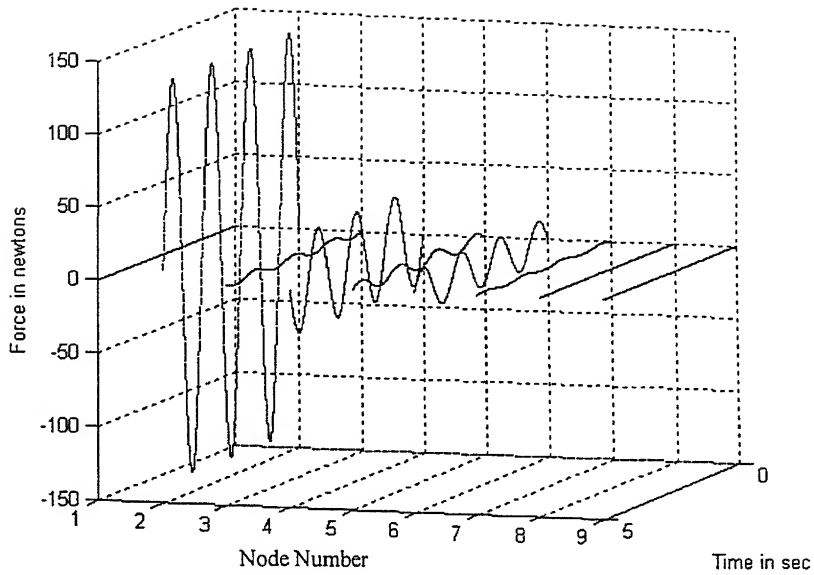


**Fig 5.5(b) Equivalent forces from experimental data**

The summary of these observations is given in Table 5.5

**Table 5.5 Summary of diagnosis for radial misalignment**

| Applied misalignment $\Delta X_L$(mm) | Identified misalignment $\Delta X_L$(mm) | Location of applied radial misalignment *(i)* | Identified Location of fault *(i)* |
|---|---|---|---|
| 0.635 | 0.456 | 2 | 2 |

## 5.6 Angular Misalignment Identification

An angular misalignment 0.0676 degree is deliberately introduced at the coupling (node 2) to carry out the experiment. Referring to the fault model for angular misalignment, given in Chapter 3 (equations 3.23), the fault vector is described by $\beta_{am}=[i \quad \Delta\varphi]^T$. The force computed from the FE model is depicted in Fig 5.6(a). The equivalent force computed from experimental data is shown in Fig. 5.6 (b).

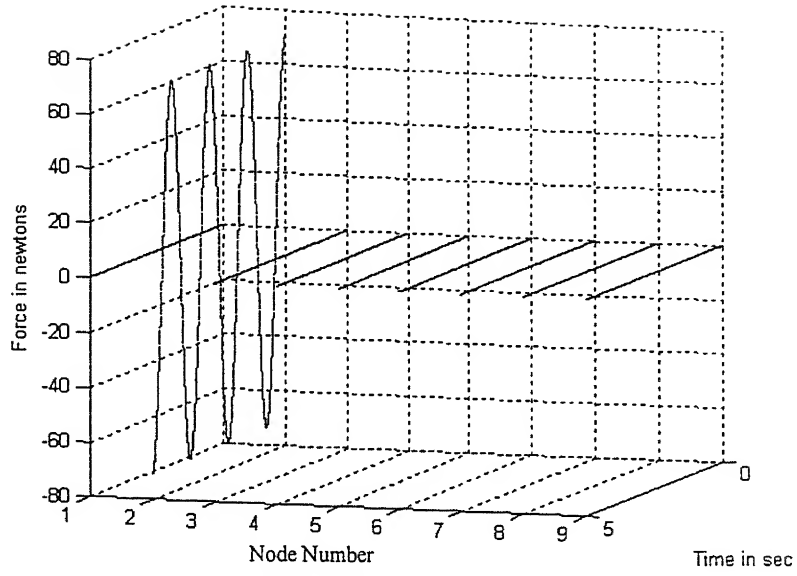


**Fig 5.6(a) FE model based equivalent forces**

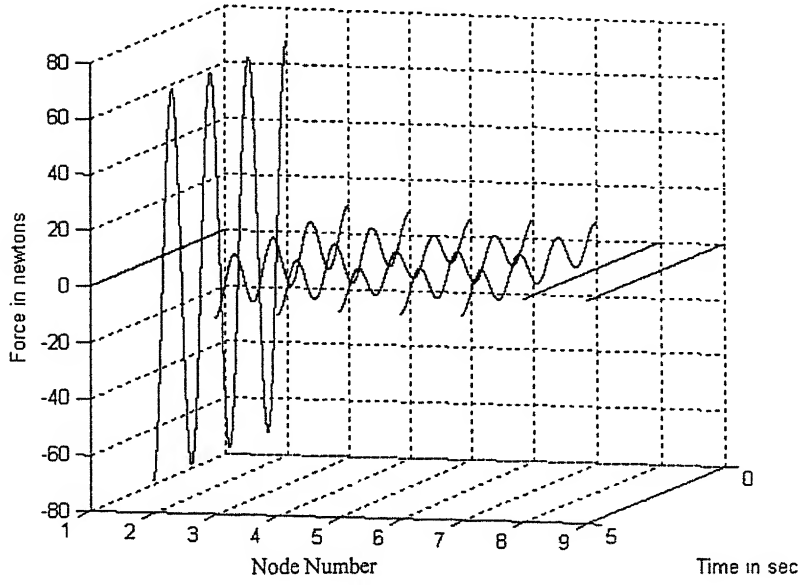


**Fig 5.6(b) Equivalent forces from experimental data**

The summary of these observations is given in Table 5.6

**Table 5.6 Summary of diagnosis for angular misalignment**

| Applied Experimentally $\Delta\varphi$ (degrees) | Identified unbalance $\Delta\varphi$ (degrees) | Location of applied angular misalignment *(i)* | Identified Location of fault *(i)* |
|---|---|---|---|
| 0.0676 | 0.0656 | 2 | 2 |

## 5.7 Identification of Rub

A residual rubbing force of 1.75 N is applied on middle of the shaft (node 5). Referring to the fault model for Rubbing is, given in Chapter 3 (equations 3.17), the fault vector is described by $\beta_{un} = [i \quad u_{rub}]^T$. The force computed from the FE model is depicted in Fig 5.7(a). The equivalent force computed from experimental data is shown in Fig. 5.7 (b).

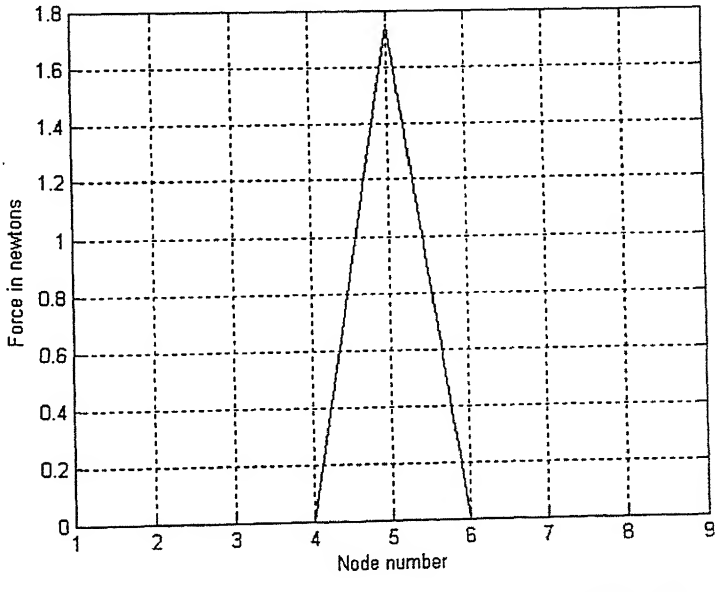


**Fig 5.7(a) FE model based equivalent forces**

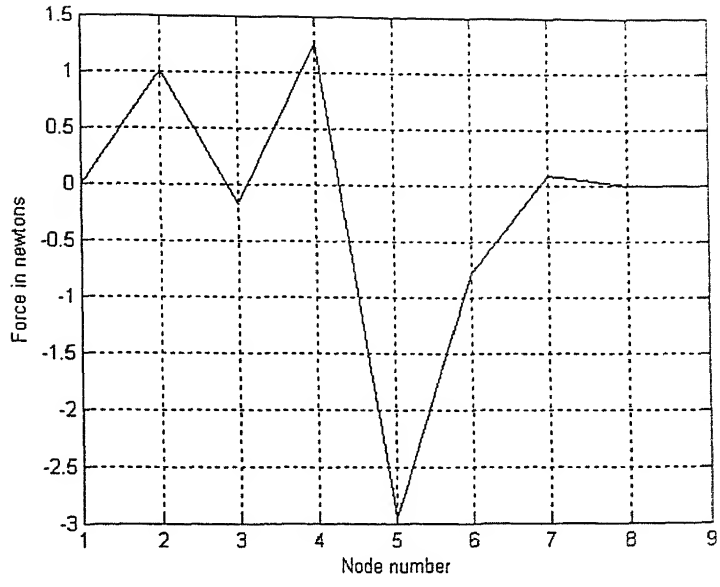


**Fig 5.7(b) Equivalent forces: Experimental**

The summary of these observations is given in Table 5.7

**Table 5.7 Summary of diagnosis for rub**

| Applied Experimentally (N) | Identified Rub (N) | Location of applied unbalance *(i)* | Identified Location of fault *(i)* |
|---|---|---|---|
| 1.75 | 2.85 | 5 | 5 |

## 5.8 Validation

In order to validate the procedure and algorithms, the above faults were introduced on the rotor in varying manners and the type, location and magnitude of the diagnosed fault were checked.

### 5.8.1 Simulation of Unbalance at Various Locations on Test rig

Normal vibrations were recorded for 2400 rpm at 5 DOFs at various locations using three proximeter sensors and two accelerometer sensors. Unbalance $u_i$ of different magnitudes are

applied at various locations on test rig. Validation results for unbalance at various locations are summarized in Table 5.8 and Figs. 5.8 - 5.10.

**Table 5.8 Summary of validation for unbalance**

| Case | Applied unbalance ($10^{-4}$)(kg-m) | Identified Unbalance ($10^{-4}$)(kg-m) | Applied location | Identified location of fault |
|---|---|---|---|---|
| 1 | 10.8 | 7.52 | Left Disk (Node 4) | 4 |
| 2 | 10.8 | 5.12 | Right disk (Node 6) | 6 |
| 3 | 10.8 | 10.34, 4.73 | Both Disks (Nodes 4,6) | 4,6 |

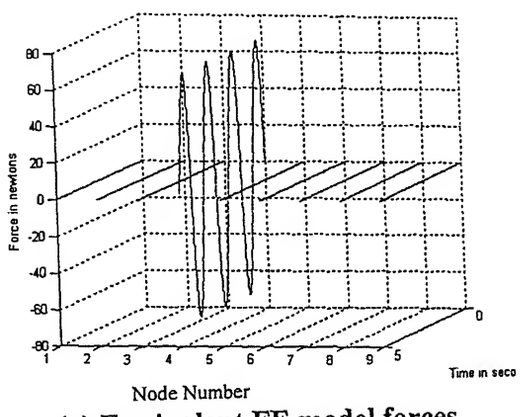


(a) Equivalent FE model forces

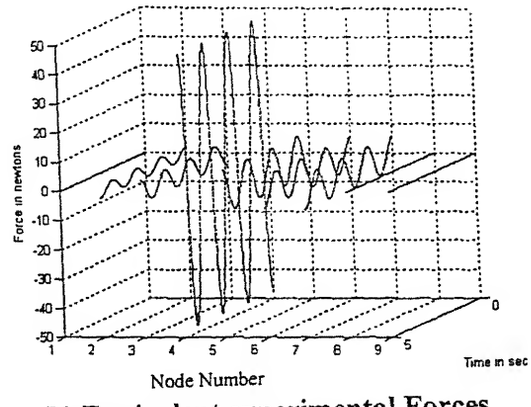


(b) Equivalent experimental Forces

**Fig. 5.8 Validation: Unbalance - Case 1 -**

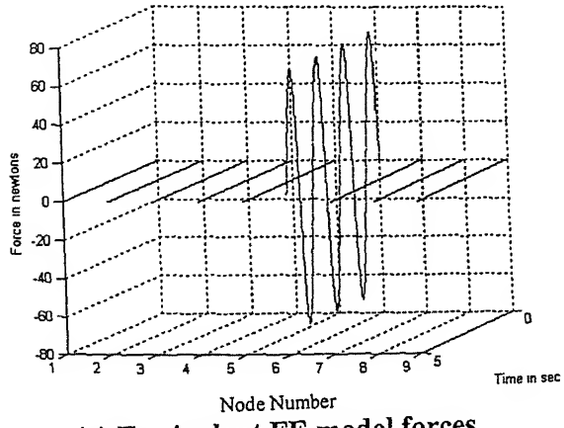


(a) Equivalent FE model forces

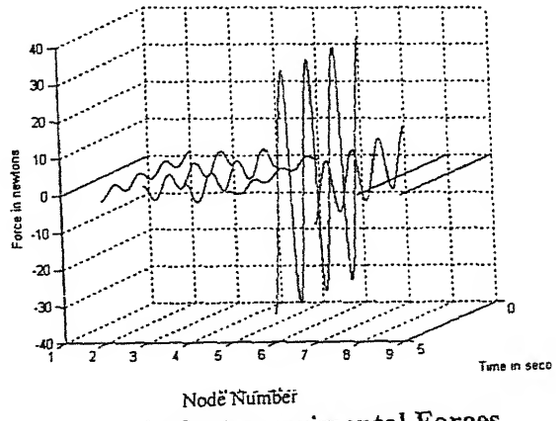


(b) Equivalent experimental Forces

**Fig. 5.9 Validation: Unbalance - Case 2**

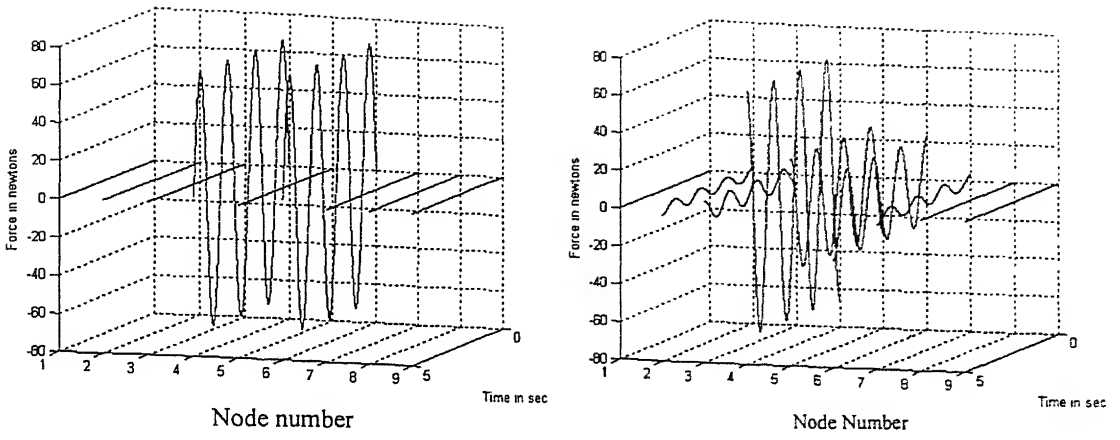


**(a) Equivalent FE model forces** **(b) Equivalent experimental Forces**

**Fig. 5.10 Validation: Unbalance - Case 3**

### 5.8.2 Simulation of Radial misalignment of various magnitudes

Summarized report of simulation of radial misalignment at various on rotor system is given in Table 5.9 and Figs 5.11-5.12.

**Table 5.9 Summary of validation for radial misalignment**

| Case | Applied misalignment(mm) | Identified misalignment(mm) | Applied fault location | Identified fault location |
|---|---|---|---|---|
| 1 | 0.102 | 0.121 | 2 | 2 |
| 2 | 0.204 | 0.305 | 2 | 2 |

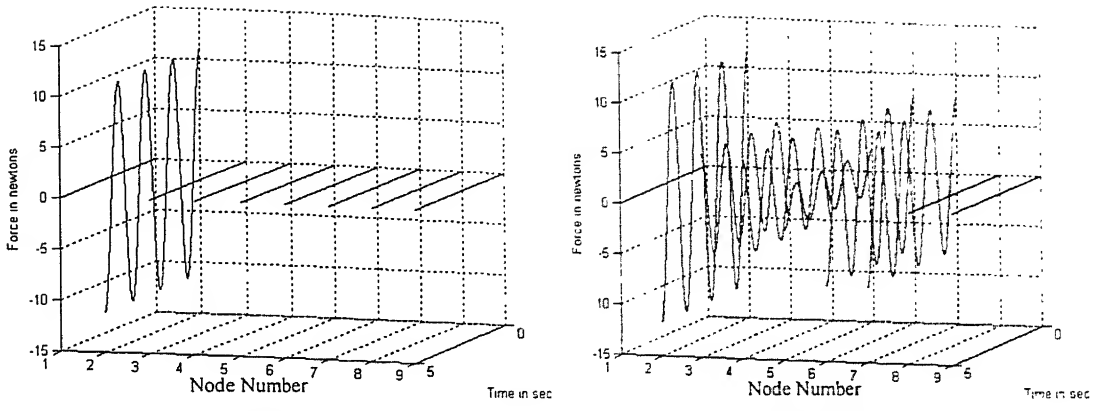


(a) Equivalent FE model forces (b) Equivalent experimental Forces

**Fig. 5.11 Validation: radial misalignment - Case 1**

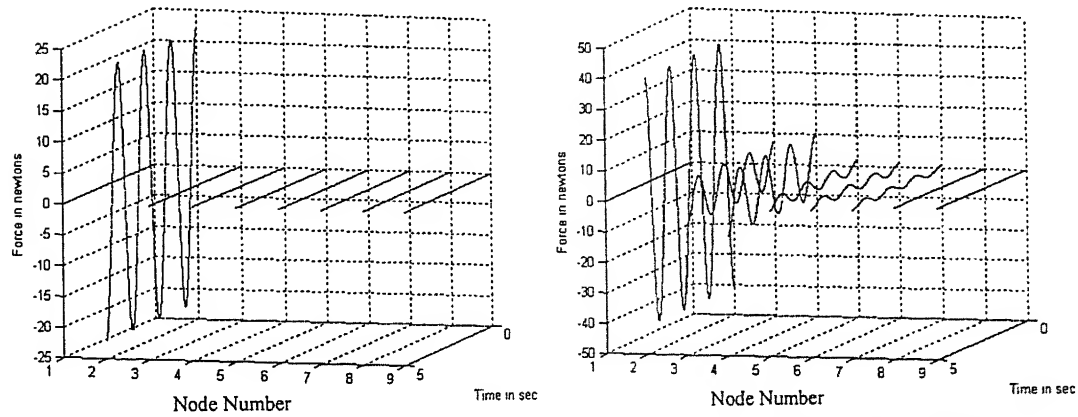


(a) Equivalent FE model forces (b) Equivalent experimental Forces

**Fig. 5.12 Validation: radial misalignment - Case 1**

### 5.8.3 Simulation of Angular misalignment of Various Magnitudes

Summarized report of simulation of angular misalignment at various locations on rotor system is given in Table.5.10 and Figs 5.13-5.14

**Table 5.10 Summary of validation for angular misalignment**

| Case | Applied misalignment (degrees) | Identified misalignment (degrees) | Applied fault location | Identified fault location |
|---|---|---|---|---|
| 1 | 0.0162 | 0.022 | 2 | 2 |
| 2 | 0.0325 | 0.0193 | 2 | 2 |

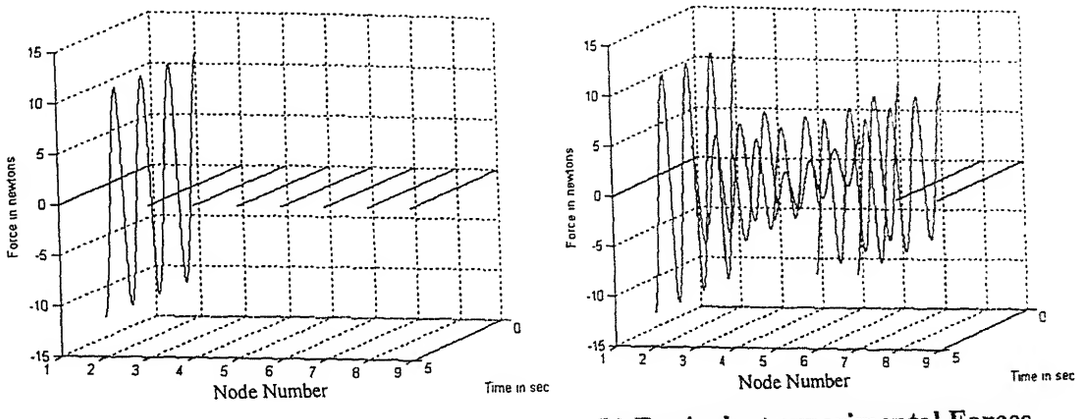


(a) Equivalent FE model forces (b) Equivalent experimental Forces

**Fig. 5.13 Validation: angular misalignment - Case 1**

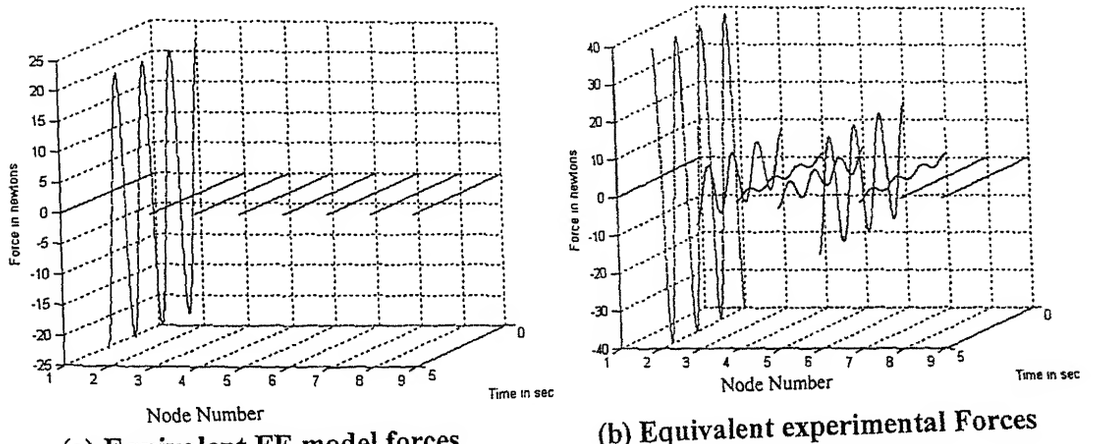


(a) Equivalent FE model forces (b) Equivalent experimental Forces

**Fig. 5.14 Validation: angular misalignment - Case 2**

### 5.8.4 Simulation of Rub at Various Locations on Test rig

Summarized report of simulation of angular misalignment at various locations on rotor system is given in Table 5.11 and Figs. 5.15-5.16

**Table 5.11 Summary of validation for rub**

| Case | Applied rubbing force (N) | Identified rubbing force (N) | Applied fault location | Identified fault location |
|---|---|---|---|---|
| 1 | 1.52 | 1.92 | 4 | 4 |
| 2 | 1.52 | 1.40 | 6 | 6 |

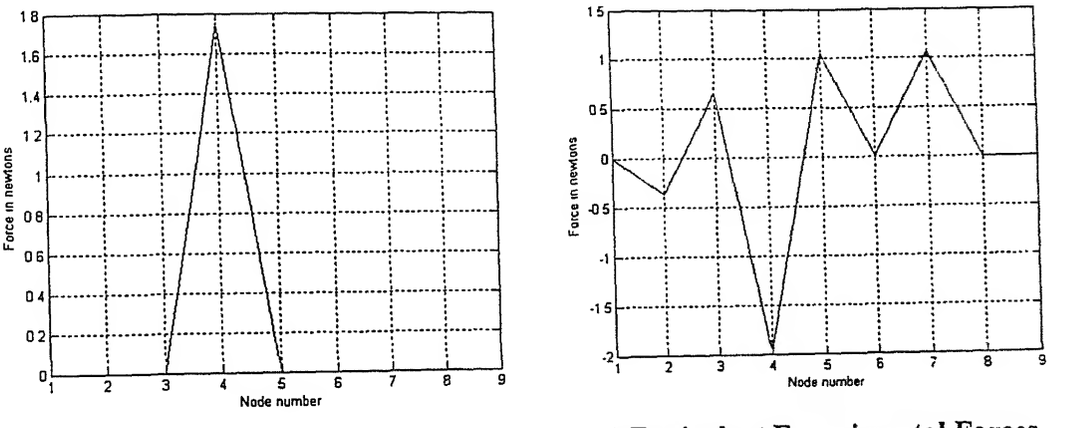


(a) Equivalent FE Model forces (b) Equivalent Experimental Forces

**Fig. 5.15 Validation: Rub - Case 2**

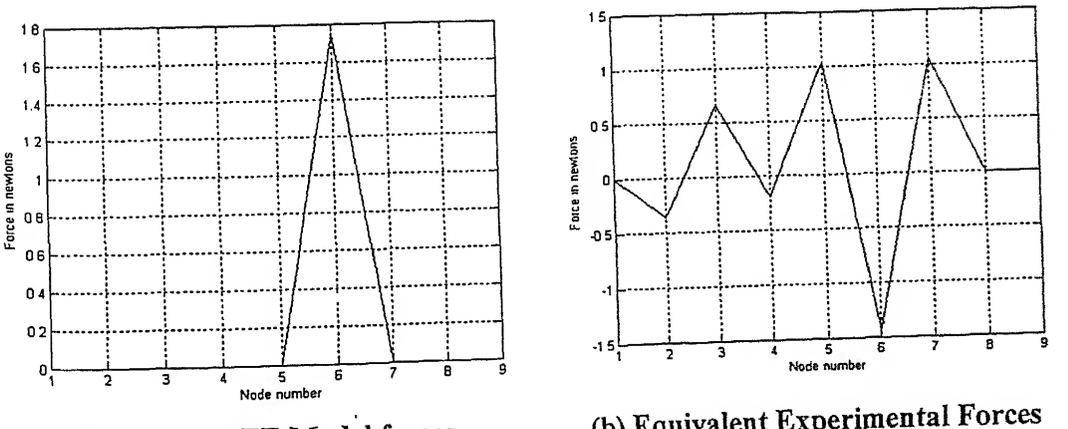


(a) Equivalent FE Model forces (b) Equivalent Experimental Forces

**Fig. 5.16 Validation: Radial misalignment - Case 2**

## 5.9 Remarks

It can be seen from the results that the model-based approach is quite efficient in diagnosing the fault. The detection of the location of the fault is always found to be correct in all the simulations carried out. The type of fault is also correctly identified. In terms of estimation of the magnitude of the fault, the algorithm performs satisfactorily to give values of the same order as the actual ones. Correct results have been obtained in the present study on the complex rub phenomenon also. The performance of the algorithm is found to be best in the case of unbalance detection. The order of error in fault magnitude estimation ranges from 11% to 25% in the case of unbalance and 26% to 38% in the case of rub phenomenon.

# CHAPTER 6

# CONCLUSIONS AND SCOPE FOR FUTURE WORK

The objective of the present work was to develop upon and implement a model based diagnostic scheme for a rotor-bearing system. The diagnosis procedure is based on mathematical model of the rotor system and representation of a fault through a virtual or equivalent force imagined to be acting on the system. This force is experimentally obtained and compared with mathematical models of the faults, through a least square error procedure.

During the present study this procedure was implemented for four different types of rotor faults. The results were validated for different locations and magnitudes of these faults. The diagnosis algorithm has been integrated with the data-acquisition hardware and software.

The procedure was found to work very efficiently in identifying the type and location of the faults, while the magnitudes of faults were estimated within an identical order of the actual ones; in other words qualitative identifications was very good while quantitative estimates were within acceptable limits. Fault quantification, however, remains a problem with other diagnosis schemes like expert system and neural networks, which work primarily with the signals, without knowledge of the mathematical model of the\system.

The model-based procedures, however suffer from the drawback of being implementable only for those faults or problems for which mathematical models exist. The number of such fault models presently is very limited. Therefore, during the course of the present study, the scheme could be implemented only for four number of faults, while it was possible to experimentally simulate many more. Also an accurate mathematical model would require sufficiently large degrees of freedom. This also necessitates an equal large number of measurement locations. The major advantage of model-based procedure was found to be its accuracy in qualitative diagnosis.

In order to explore the full potential of such a procedure activity needs to be undertaken in two areas – (i) mathematical modeling faults and fault combinations and (ii) optimization of the number of sensor locations.

# REFERENCES


1. Ankur, "Real Time Condition Monitoring of Rotors using Self Organizing Maps". M. Tech thesis, 2003, IIT Kanpur
2. Bach, H., Markert, R., 1997. "Determination of the fault position in rotors for the example of a transverse crack. Structural Health Monitoring", Technomic Publishers. Lancaster, 325.
3. Bachschmid, N., Pennacchi, P., Vania,A, 2001."Identification of multiple faults in rotor systems". Journal of Sound and Vibration V 254 (4), 327
4. Eisenmann R.C. Sr., Eisenmann R.C. Jr., "Machinery Malfunction Diagnosis and Correction", Prentice-Hall PTR, New Jersey, 1998.
5. Jain, J.R, Kundra, T.K, 2003 "Identification of Unbalance and Transverse Cracks in rotor Systems" Mechanics Research Communications, Article in press
6. J.N.Reddy, "An Introduction to The Finite Element Method", second edition , Tata McGraw-Hill, New Delhi, 2003
7. Jimin He, Zhi-Fang Fu., "Modal Analysis". First edition, Butter Worth Heinemann, New Delhi,2001
8. Markert, R., Seidler, M., Platz, R., 2001. "Model based fault identification in rotor systems by least square fitting". International Journal of Rotating Machinery. 246 7 (5), 311.
9. Padhy, M.V, "Fault Identification in Rotating Machinery using Neural Networks and Virtual Instrumentation". M. Tech thesis, 2001, IIT Kanpur
10. Platz, R., Markert, R., Seidler, M., 2000. "Validation of online diagnostics of malfunctions in rotor systems", In: Transactions of Seventh IMechE Conference on Vibrations in Rotating Machinery, University of Nottingham, UK, 571.
11. Rao, M.V, "Neural Network Applications for Rotating Machinery Fault Diagnosis" M. Tech thesis, 2002, IIT Kanpur
12. Rao J.S., "Rotor Dynamics", Third edition, New Age International (P) Limited, New Delhi, 1996
13. Sekhar, A.S., Prabhu, B.S., 1992. "Transient analysis of a cracked rotor passing through critical speed". Journal of Sound and Vibration 173 (3), 415.

A 148418

**Date Slip**

This book is to be returned on the date last stamped.

| | |
|---|---|
| ..... | ..... |
| ..... | ..... |
| ..... | ..... |
| ..... | ..... |
| ..... | ..... |
| ..... | ..... |
| ..... | ..... |
| ..... | ..... |
| ..... | ..... |
| ..... | ..... |
| ..... | ..... |
| ..... | ..... |